A QUANTUM MECHANICAL STUDY OF HYDROGENATED SILICON CLUSTERS USING GENETIC ALGORITHM

by

PARTHA SARATHI DE

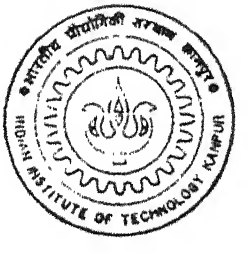

MATERIALS AND METALLURGICAL ENGINEERING

Indian Institute of Technology, Kanpur

DECEMBER, 1998

A QUANTUM MECHANICAL STUDY OF HYDROGENATED SILICON CLUSTERS USING GENETIC ALGORITHM

A Thesis Submitted

in Partial Fulfillment of the Requirements

for the Degree of

Master of Technology

by

PARTHA SARATHI DE

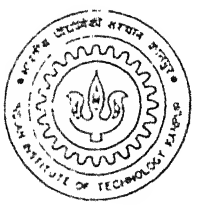

to the

MATERIALS AND METALLURGICAL ENGINEERING
INDIAN INSTITUTE OF TECHNOLOGY KANPUR

DECEMBER 1998

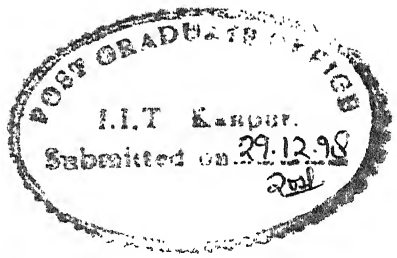

CERTIFICATE

It is certified that the work contained in this thesis entitled "*A Quantum Mechanical Study of Hydrogenated Silicon Clusters Using Genetic Algorithm*", by *Partha Sarathi De*, has been carried out under my supervision and that this work has not been submitted elsewhere for any degree.

N Chakraborti

Dr. N. CHAKRABORTI
Professor
Materials and Metallurgical Engineering,
Indian Institute of Technology, Kanpur
December, 1998

Acknowledgement

I sincerely thank Prof. N. Chakraborti for initiating me into this interesting field of amorphous silicon. His widespread knowledge in genetic algorithm coupled with his skillful guidance has paved the way to my understanding in this subject. It is needless to say that without his help this work may not have been done.

My sincerest thanks are also due to Prof. R. Prasad and Dr. G.R. Gupte of Physics department, for providing me total support in implementing the most important part of cohesive energy calculation.

Thanks are also due to Mr. Nazrul Islam, of Physics department and Mr. Atanu Saha of Materials Science programme for the valuable help rendered during my thesis work.

Abstract

Silicon forms the backbone of modern electronic industry. The crystalline state of this element in its pure or impure form, is the most commonly used material. However other forms of silicon are also increasingly finding their use, and have already established a niche for themselves. Thus amorphous silicon passivated with hydrogen (a-Si:H) has emerged as a popular optoelectronic material with widespread application in solar photo-voltaic industry. The material has also revolutionized the growth of microelectronics with applications in LCD/TFT's and light sensors. But inspite of the increasing technological implications of this material, not much is known about its physics. The issues of thermal instability, sensitivity to visible radiation, affecting the properties of a-Si:H are yet to be understood.

In this study we have focussed our attention on hydrogenated clusters of silicon. Clusters constitute an assortment (from 2 to 100) of silicon atoms in association with hydrogen. They exhibit markedly different material properties from bulk silicon with potential application in cluster assembled material. Moreover a study of these clusters is expected to throw light on the Staebler-Wronskii effect exhibited by a-Si:H. Implications also exist in the realm of porous silicon another futuristic material with potential application in LEDS and semiconductor lasers. Amorphous silicon and porous silicon together has raised the hope of producing integrated opto-electrical circuits.

Calculating the ground state geometry of clusters was the principal objective of this study. This constitutes in optimizing structures of clusters generated randomly, using genetic algorithm. The cohesive energy of cluster comprised of our objective function. A confined

cubic space with specified dimension was chosen (Cubic box with dimension 4 to 7Å) wherein the cluster evolves, giving the final ground state configuration. Thus for a n atom cluster the total number of variables to be optimized is $3n$, consisting of x, y, z, coordinates for each atom. The lower and upper bounds of each variable is given as $0 \leq x_i \leq$ L where L is the length of cube side.

The cohesive energy of a cluster is calculated using the principles of Non-orthogonal tight binding theory. According to this theory, cohesive energy of a system comprises of two principal parts: a classical contribution, consisting of coulombic interaction between atoms and a quantum part involving electronic interaction in the atoms itself. This particular methodology was chosen since it is both accurate and also computationally efficient. It is especially true for the Si-H semiconductor system. In this work we have presented the optimized structures of a number of a-Si:H clusters for Si_nH_m (n = 1-2, H = 1-5) and Si_kH (k = 3-8) varieties.

Contents

List of Figures

List of Tables

Chapter 1

Introduction

Hydrogenated amorphous silicon (a-Si:H) is increasingly becoming an important material, emerging a long way from its initial beginning as a potential candidate for solar cell applications [1]. Since then interest in the material has grown up rapidly with its application extending into the field of large area microelectronics, sensors, detectors etc. The various advantages of amorphous Si-H and its alloys are discussed below

- Short optical absorption length for visible light.
- Good intrinsic and doped semiconductor properties.
- Deposition easily at low cost over extremely large areas. The temperature of deposition is low and is of the order of 250 ^{o}C.
- Monolithic integration of individual cells is simple which avoids costly cut and paste methods.
- Both silicon and hydrogen are abundant material constituting more than 50 -60% of the earths crust.

Due to the above mentioned qualities a-Si:H has become the most used thin film material for photo-voltaic cell constructions and as contact image-sensors in scanning machines. A schematic diagram of a contact image-sensor is shown in Fig. 1.1 [2].

The ability of a-Si:H sensors to copy over large paper width, high resolution of imaging and simplicity in optical system design, has made them useful for document scanning.

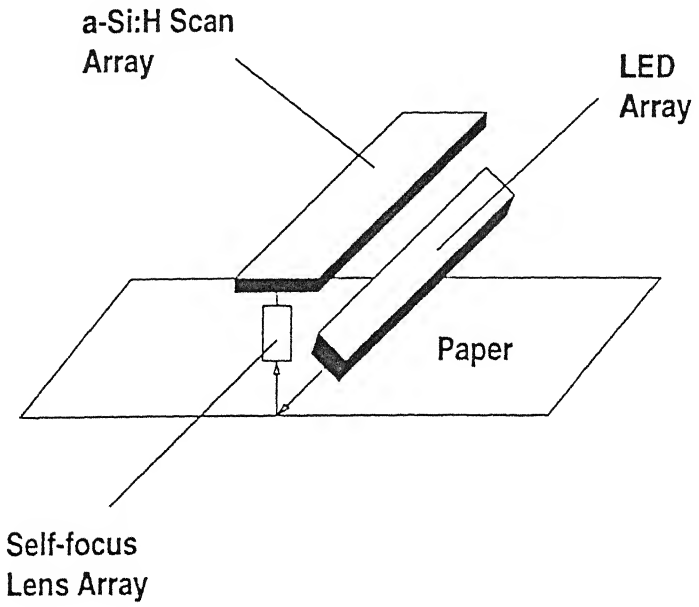

Figure 1.1: Schematic of electrophotographic sensor (Source: [2])

Due to their high sensitivity to long wavelength visible light, high dark resistivity and strong resistance to mechanical wear, a-Si:H alloys have also been used as photo-receptors for electro-photography. Their first commercial use in electrophotographic drums was done by Canon Inc. in 1984. The smaller band gap of a-Si:H alloys compared to amorphous selenium allows a shorter discharge time, which implies higher copying speed. In electrophotographic processes the thickness of a-Si:H films required is of the order of 20μm. This requirement of thickness is an important issue to be considered since the deposition rates of high-quality a-Si:H films are below 0.4 nm/s.

Amorphous Si:H has also found its utility in photodiode applications like ultraviolet light, X ray and charged particle detectors, as image sensors for neural network applications [3] etc.

The advantages of producing uniform film coatings, high yield and considerable field effect mobility offered by a-Si:H, has established it as an ideal material for large area electronics applications. A widely used application of a-Si:H is in the fabrication of thin film

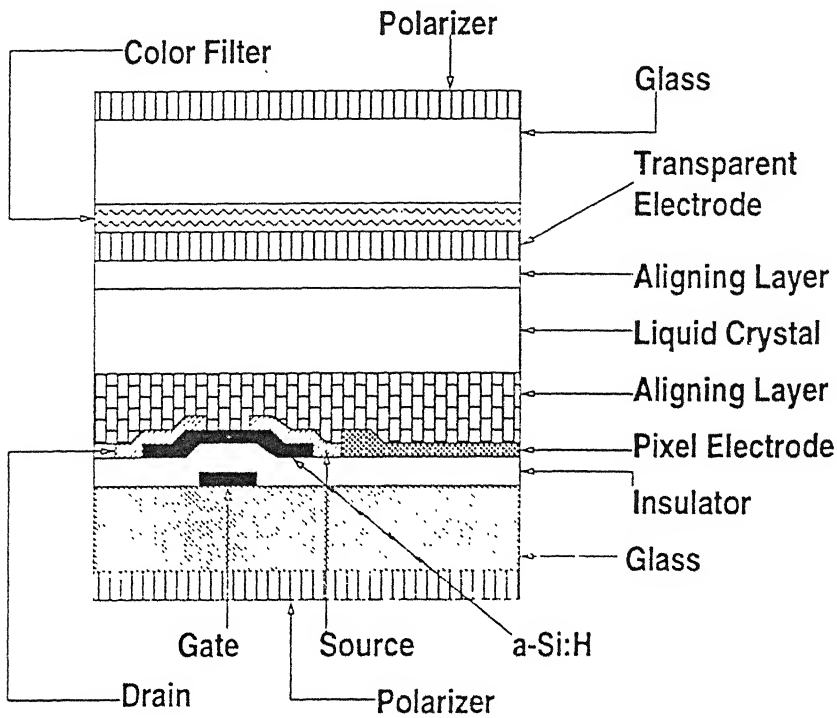

Figure 1.2: Cross-Section of an a-Si:H / color Display (Source: [4])

transistors (TFT) used in controlling liquid crystal displays (LCD) [4]. A schematic of such a device is given in Fig. 1.2. Presently this technology is heavily used for the manufacture of portable television and in military/avionic applications.

The fast progressing technology of a-Si:H is however plagued by its own characteristic problem. All amorphous Si:H alloys exhibit reversible degradations in many material characteristics on being subjected to light exposure, charge injection or thermal quenching. Understanding the physics behind these phenomenon is therefore becoming increasingly important to give rise to a more reliable technology. In the next section we have outlined, the common techniques used for producing device quality a-Si:H.

1.1 Production of a-Si:H Based Materials

The different deposition techniques for a-Si:H are [5].

- Chemical vapor deposition technique which includes , PECVD, PACVD etc.
- Reactive sputtering.

However the chemical vapor deposition technique employing glow discharge is the most popular method. In this method the starting gas material used is generally silane (SiH_4). This gas (also known as carrier gas) is introduced at a controlled rate in between two electrodes in a evacuated gas chamber, where it is subjected to glow discharge produced by initiating a direct current (DC) or alternating current (radio frequency or microwave). The discharge causes the gas to dissociate and ultimately get deposited on a substrate producing a-Si:H film. A simplified diagram of the glow discharge process is given in Fig. 1.3.

1.2 Staebler-Wronskii Effect

Staebler and Wronskii [6] reported that a-Si:H films on being exposed to visible radiation shows an alteration in their material properties. Thus the properties of dark conductivity and photo-conductivity in a-Si:H show a diminishing trend on being exposed to light. This effect is stable at room temperature, but is reversed to its original state on annealing treatment at 180 ^oC for a time period of one to two hours. Treatment of the film by infrared light however fails to restore its initial state. Ever since the discovery of this phenomenon lot of research work has been done to get a clear understanding of this effect. As of now no universally accepted model for the underlying mechanism has been found. However some of the widely accepted experimental facts in this regard are given below [7].

- This light-induced degradation is observed in all a-Si:H films regardless of its method of preparation and film quality.
- The phenomenon is a bulk effect.
- Light soaking with photon energy larger than 1.1 ev, can all induce this effect. Thus

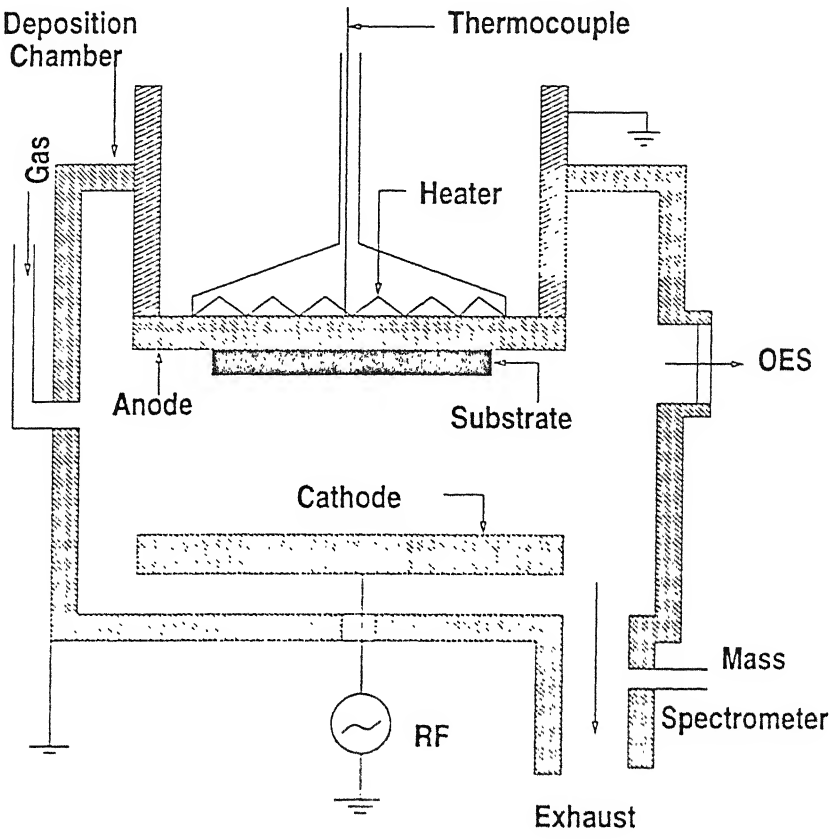

Figure 1.3: Schematic of glow-discharge deposition process

bombardment by high energy particles, quenching from high temperatures, charge injection etc., have a similar effect on a-Si:H.

- The effect decreases with the decrease of sample temperature.
- The defect can be removed by thermal annealing at 100 to 200 ^oC for about one hour. Infrared radiation has no effect on the process of annealing; visible light however increases the annealing rate.
- Neutral silicon dangling bonds formed during the creation of this metastable state are situated 0.8 ev above the valence band mobility edge.
- The metastability is proposed to be an intrinsic property of a-Si:H alloys, since impurities below $1*10^{18}$ cm^{-3} have no detectable effects [8]. It is worthwhile mentioning here that

concentration of most impurities, like P, B, C, and N, can be reduced to levels lower than the concentration of light-induced defects without improving the stability of the material.

• The phenomenon is not directly related to any intrinsic mechanical stresses generated during the film preparation stage [9].

Several models for the microscopic mechanism of metastability in a-Si:H alloys have been proposed. Some of the well known models are [7]

1. Weak-bond-breaking model [10, 11, 12].
2. Charge-defect model [13, 14, 15].
3. Rehybridized two-site model [16].

Most of the models involve the presence of hydrogen in the material. Experimental relationship between the diffusion coefficient of hydrogen and annealing rate has also been established. All this warrants a fundamental understanding about the molecular structures and internal bonding of a-Si:H, in particular. Furthermore, identifying the controlling reactions in the production of hydrogenated amorphous silicon involves a thorough knowledge about the various Si-H clusters and their relative stability. In this work we focus on Si_nH_m (n = 1,2 and m = 1,5) and Si_kH (k= 3,8) clusters.

In an earlier study, based upon non-orthogonal tight binding molecular dynamics model [17], Gupte and Prasad [18] reported the ground state structures and the vibrational spectra of these clusters using the simulated annealing technique. Although a large number of structures were obtained during that work, the requirement of large CPU time often renders the usage of simulated annealing in such problems computationally prohibitive. Our main aim in this work is to replace simulated annealing by genetic algorithm (GA) [19] in order to calculate the ground state structures with better efficiency. The computational gains using GA can be extended further with the parallelization of our code. It is worth mentioning here that, GA is highly suited for parallel processing unlike any other traditional or non-traditional optimization methods. In the next chapter the fundamentals of GA are discussed.

Chapter 2

Fundamentals of Genetic Algorithm

Traditional optimization methods are derivative based. Starting from an initial guess, the search algorithm selects a new point based upon some derivative criteria, leading to the nearby optimum. Extensive details on traditional optimization methods are available elsewhere [20]. However in genetic algorithm the approach is entirely different in that a set of initial points, *individuals* in GA parlance, is the starting point. These group of individuals *population* in GA terminology are generally subjected to three powerful genetic operators: *reproduction*, *crossover* and *mutation* [19] described later. The basic principle of genetic algorithm is based upon the quasi-Darwinian principle of survival of the fittest where an individuals claim to pass its clone to the next generation is evaluated in terms of its fitness, which is either the function itself or some appropriate transformation of it. For example, in order to optimize a function ϕ(x) between the lower and upper bounds x^L and x^U, the fitness function f(x) can be taken identical to ϕ(x) in a maximization case. On the other hand, in a minimization problem, the fitness function can be defined as

$$f(x) = \frac{1}{1+\phi(x)} \tag{2.1}$$

Several other suitable transformation of the objective function can be taken depending upon the nature of problem to be solved. In GA the variables are generally coded as binary strings

using '1's and '0's. Thus if four bits are used to code the variable x, then the strings (0000) and (1111) would represent x^L and x^U respectively, since those are the strings having the minimum and maximum decoded values. To convert the binary variables to real, different transformation schemes are used. A commonly used rule is linear mapping which is stated as:

$$x = \frac{x^U - x^L}{2^l - 1}(S) \tag{2.2}$$

In the above equation S is the decoded value of the binary string s of length l, representing the variable x. If the j'th bit in the string is denoted by s_j, then

$$S = \sum_{j=0}^{l-1} 2^j s_j \quad \text{where} \quad s_j \epsilon (0, 1) \tag{2.3}$$

Thus the four-bit string (1111) has a decoded value of 16. All the variables representing a point are mapped onto their binary equivalents which are concatenated together to form a single string whose fitness is then calculated. Using the initial population one then proceeds to create a mating pool consisting of individuals selected on the basis of their fitness values. The reproduction operator is used for this purpose. A detailed discussion on the various mechanisms of reproduction are given below.

2.1 Reproduction Operators

Initially reproduction (or selection) operator is applied on a given population. The consequence of this operation is to select the higher fitness strings, which together create the mating pool. These strings in the mating pool are then subjected to crossover and mutation processes before being passed into the next time step, *generation* in GA terminology. As in this real world, an individual in GA is subjected to the same phenomena of birth and death which can be expressed mathematically as [21]

$$I_{k,t+1} = I_{k,t} + I_{k,t,b} - I_{k,t,d} \tag{2.4}$$

Here I denotes the number of individuals with the same fitness f_k, 'k' being its fitness class identifier, while 't' is the time at which the class is considered. The subscript 'b' denotes the individuals being born in that class while 'd' symbolizes those dying. In a normal scheme (also known as overlapping population model) all the individuals existing in the present time step is considered to die, birth rate being the sole criteria determining the number of individuals existing in that class at the next generation. One of the more commonly used selection operator is the fitness proportionate selection method. Here the probability of selecting an individual of the the i'th class into the mating pool can be approximately given as

$$p_i = \frac{f(x_i)}{\sum_{j=1}^{n} f(x_i)} \tag{2.5}$$

Goldberg and Deb [21] have shown that for a non-overlapping population of constant size n the expected number of copies of i'th class (among a total of k classes) in the following generation is given by

$$P_{i,t+1} = P_{i,t}\frac{f_i}{\bar{f}_t} \tag{2.6}$$

where $\bar{f}_t = \sum m_{i,t} f_i / n$, is the average function value at the current generation, n being the population size. Solving equation (2.6) we get [21]

$$P_{i,t} = \frac{f_t P_{i,0}}{\sum_j f_j^t P_{j,0}} \tag{2.7}$$

In order to have an understanding about the convergence situation, Goldberg and Deb [21] undertook an analysis for the takeover time required by this selection method; takeover time being defined as the time required by an individual of the best group to acquire a $\frac{n-1}{n}$ pro-

portion of the total population. Considering a polynomial objective function the calculated takeover time is found to be [21]

$$t^* = \frac{1}{c}(n \ln n - 1) \tag{2.8}$$

c being the exponent of the functions considered and is a constant. For an exponential function the takeover time is given as

$$t^* = \frac{1}{c} \ln n \tag{2.9}$$

Thus for exponential objective functions the proportionate distribution method converges in O(ln n) time, a factor of n faster than that required in the polynomial case. However a major problem in using this type of reproduction operator is premature convergence. During the initial time fitness variance in the population is high, with few high fitness strings while the remaining being of much lower fitness. On using this mechanism of reproduction the higher fitness strings propagate quickly resulting in a lack of diversity in the population [22]. Avoidance of such problem involves the usage of low selection pressure at the initial period when population variance is high and increasing the pressure at a later time period when the variance decreases.

Sigma scaling technique incorporates this mechanism. Here an individual's expected value is expressed as a function of its fitness, population mean, and the population standard deviation. An example of sigma scaling is given below [22]

$$Exp\,Val(i,t) = \begin{cases} 1.0 + \frac{\text{f(i) - } \bar{f}(\text{t})}{2\sigma(\text{t})} & \text{if } \sigma(\text{t}) \neq 0 \\ 1.0 & \text{if } \sigma(\text{t}) = 0 \end{cases} \tag{2.10}$$

where $Exp\,Val(i,t)$ is the expected value of individual i at time t, f(i) being the fitness of i, $\bar{f}$(t) the mean fitness of the population at time t, and σ(t) the standard deviation of the population fitness' at time t.

Rank selection operator is another selection methodology where an individual is selected on the basis of their ranking. The takeover time for linear ranking scheme [21] is given as

$$t^* = \frac{2}{c} log(n-1) \tag{2.11}$$

In ranking selection the procedure involves sorting the entire population according to their individual fitnesses which is done on the basis of some assignment function. This kind of selection technique has been identified to be potentially time consuming, specially when the population size involved is large [22].

To avoid this disadvantage the tournament selection operator is the most appropriate method. It includes the advantage of rank selection operator in maintaining a uniform selection pressure and is computationally much more efficient being well suited for parallel processing. The implementation involves selecting two individuals randomly from the given population which are then allowed to compete against each other. A uniform random number is generated between 0 and 1 which is then compared to a parameter k; if the number is greater than k, the fitter individual is selected or otherwise. The tournament selection method is sometimes associated with *Elitism* where the fitter individual is selected preferentially. It maybe mentioned here that tournament selection with more than two competitors has also been devised.

Goldberg and Deb [21] has solved the takeover time for tournament selection which is expressed as

$$t^* = \frac{1}{\ln s}[\ln n + \ln(\ln n)] \tag{2.12}$$

where s is the tournament size.

Of the different reproduction operators stochastic universal proportionate, stochastic remainder proportionate and tournament selection algorithms are the only ones with a O(n)

time complexity and are the recommended selection operators [21]. In our work we have used the binary tournament selection operator. The string with higher fitness was selected, the process being repeated 'n' times 'n' being the population size. In genetic algorithm, unlike in natarul biological systems, the population size is kept constant throughout. The essential idea of reproduction is to assign more copies of the string with higher fitness to the *mating pool*, consisting of selected individuals where the crossover and mutation operators are applied with a pre-assigned probability. Detailed discussion on the crossover mechanism is given below.

2.2 Crossover

Single-point crossover is the technique commonly used by GA researchers. Here two strings are randomly chosen from the mating pool. For example in a six-bit population:

110100

and

001011

could be two typically selected individuals. Next, a uniform random number between 0 and 1 is generated. If the random number is less than a pre-assigned probability, the process of crossover is activated by selecting a random crossover site (|) and swapping the bits right to it. For example, if the random crossover site is after the third bit from the right hand side, such that

110 | 111

001 | 011

then the crossover process results in the offsprings

110011

and

001111

In GA literature the above mentioned crossover procedure is known as single point crossover. Another variant of crossover is the two-point crossover technique. Here two crossing sites are chosen at random and the segments between them exchanged. Thus consider the two strings with their crossing site as given below

11 | 01 | 11

00 | 10 | 11

After crossover the two new strings generated are

111011

000111

As an extension of the two-point crossover technique multi-point techniques have also been developed. Uniform crossover method is a multi-point technique stretched to its extreme. Here each bit of the individual is exchanged with a probability 'p'. The value of 'p' is generally kept in the range 0.3 - 0.5.

The selection of proper crossover technique is very important. However no simple solution exists to predict the proper choice of crossover technique, the issue being variously determined by the nature of function used, variable coding and other GA parameters. In a comparative analysis of different crossover techniques [22] the two point crossover method has been preferred. The single point crossover technique is said to be more prone to positional bias and endpoint effect. This occurs as a consequence to the fact that single-point crossover favors the formation of short schema [1] which is invariably accompanied by the preservation of unfavourable bits associated with short range schemata's. Besides, in single point mechanism the string ends are always exchanged during crossover. The experiments with Royal Road functions have also shown up these effects [22]. However it would be inappropriate to make a deterministic view about the choice of crossover techniques from empirical evidences obtained from test runs on a specific function. The uniform crossover method on the other

[1]Schema (Schemata in plural) represents the commonality in bit positions among a group of strings. Thus in a three bit problem, the (10*) schema, displays the similarity among the (100) and (101) strings. For further reference check [19].

hand is free from positional bias but at the same time is highly disruptive to schema formation mechanism [22]. Theoretical studies on the search power of uniform crossover with its extension to more complicated cases are available in [23].

In the present study both single and two-point crossover methods have been applied. Uniform crossover technique was also applied, but was found to be inferior with respect to the performance of single and two-point methods.

2.3 Mutation

After crossover the mutation operator is applied. The idea is to facilitate a local search by sparingly altering some of the bits. Mutation operator therefore examines each binary bit of an individual, and attempts to change it to its complement with a small pre-assigned probability. While examining any particular bit, a uniform random number is generated. If the random number is less than the mutation probability, the bit is changed to its complement. New strings created at the end of these processes are evaluated for their fitness'. The mutation process described above is known as *jump mutation*; another variant called *creep mutation* is also used. In creep mutation each variable is examined in the real space, and is either increased or decreased by a small value with a probability of 0.5 which is then reconverted into the binary space.

After the process of mutation is over the new strings obtained are evaluated for their fitness' which completes a cycle of GA iteration. The same procedure is continued until a terminating criterion is satisfied. In the next few sections some advanced operators used in GA are discussed.

2.4 Niching

In biological terms niche can be explained as an organism's job or role in an environment [19]. The importance of niching in the light of function optimization is discussed here. Let

us consider a function as shown in Fig. 2.1 which we want to optimize using a simple genetic algorithm. We begin with a random population on which the genetic operators of reproduction, crossover and mutation is applied. It is likely that in such a case the population will tend to converge onto one of the peaks shown. This is principally due to the so called genetic drift resulting from stochastic errors caused by small population sizing [19]. Alternately a optimization problem can lead to a function exhibiting multi-modality with different peak heights. In many practical cases we are interested in identifying all the relevant peaks which is otherwise impossible to do using traditional optimizers, at least in a single run. The technique of niching in genetic algorithm plays a major role in this regard.

A number of techniques exists to implement the niching scheme in genetic algorithm. Gold-

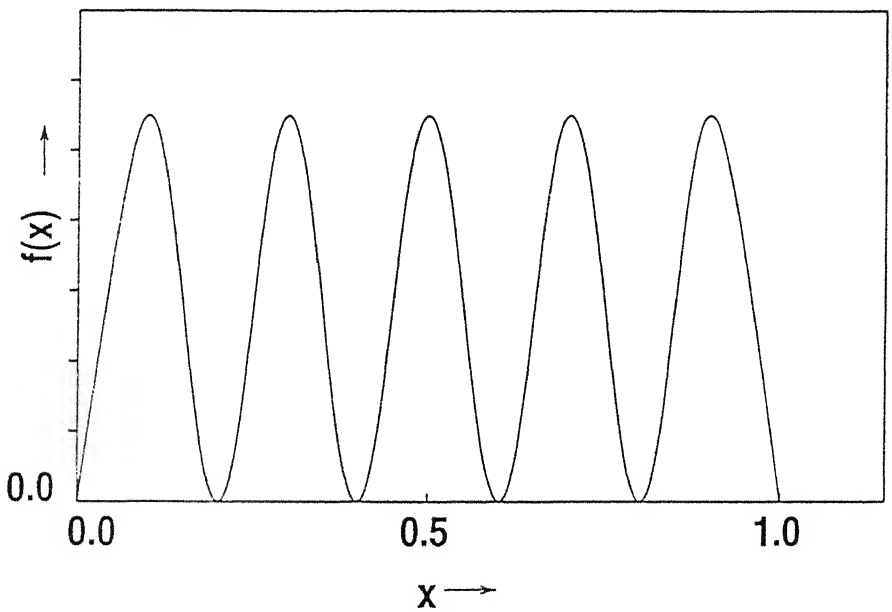

Figure 2.1: Function showing equal peaks (Source: [19])

berg and Richardson [24] utilized this concept by introducing the sharing function. Here the population is divided into different sub-populations according to the similarity of the

individuals [25]. This can be done either in the real space or even in the binary space itself. When the implementation is done on the real space it is called *Phenotypic Sharing*, and in binary space it is known as *Genotypic Sharing*. A parameter σ_{share} [24] is constructed, which determines the sharing existing between the strings. The power-law sharing function *Sh(d)* is then defined as [25]

$$Sh(d) = \begin{cases} 1.0 - (\frac{\mathrm{d}}{\sigma_{share}})^{\alpha} & \text{if d} < \sigma_{share} \\ 0.0 & \text{if d} \geq \sigma_{share} \end{cases} \tag{2.13}$$

where d is defined as the distance between two individuals. Once the extent of sharing is determined an individual's fitness is degraded accordingly. The working of the sharing principle depends chiefly on the parameter σ_{share} the choice of which is vital [25]. The parameter σ_{share} depends on the number of peaks and the lower and upper bounds of the solution space [25].

2.4.1 Phenotypic Sharing

In this type of sharing the distance (d_{ij}) between the strings can be calculated using any appropriate *distance norm* in the n-dimensional space [25]. The Eucledian distance in the n-dimensional space can also be adopted [25] and is given as

$$d_{ij} = \sqrt{\sum_{k=1}^{n} (x_{k,i} - x_{k,j})^2} \tag{2.14}$$

where $x_{1,i}$, $x_{2,i}$,.....$x_{n,i}$ are the parameter values in the real space for the 'i'th individual.

For estimating the parameter σ_{share} each niche is considered to be enclosed in a n-dimensional hyper-sphere of radius σ_{share} such that each sphere encloses $\frac{1}{q}$ of the volume of the solution space, q being the total number of peaks existing [25]. The radius of a hyper-sphere enclosing the entire space is then given as

$$r = \frac{1}{2}\sqrt{\sum_{k=1}^{n}\left(x_{k,max} - x_{k,min}\right)^2} \tag{2.15}$$

the volume of sphere being calculated as V = cr^n where c is a constant [25]. Thus σ_{share} is then calculated as given below [25]

$$c\sigma_{share}^n = \frac{1}{q}cr^n \tag{2.16}$$

$$\sigma_{share} = \frac{\sqrt{\sum_{k=1}^{n}\left(x_{k,max} - x_{k,min}\right)^2}}{2\sqrt[n]{q}} \tag{2.17}$$

2.4.2 Genotypic Sharing

In genotypic sharing the genetic proximity between two individuals is defined by the number of different alleles in their chromosome [25]. Thus consider two strings s_i and s_j both of string length l. Comparing the two given strings, if only one bit difference is allowed between them then ${}^lC_1$ is the total number of allowable strings. Thus for k allowable bit differences the total number of possible strings are ${}^lC_k$. As the total number of allowable strings in the binary space is 2^l so proportion of strings which are k bits different is ${}^lC_k/2^l$ of the given solution space. Thus the total proportion of strings with k bit differences or less is given by the expression $\sum_{i=0}^{k} {}^lC_i/2^l$. Now assuming that the function considered has q peaks distributed uniformly in the entire variable domain, each niche should then correspond to an average of $\frac{1}{q}$ of the total solution space. Thus k being the maximum allowable bit difference, therefore

$$\frac{1}{2^l}\sum_{i=0}^{k} {}^lC_i = \frac{1}{q} \tag{2.18}$$

2.4.3 Triangular Sharing Function

In the present study Goldberg's triangular sharing function has been used (see Fig. 2.2). In this method the difference in distance between each parameter to be niched is found out

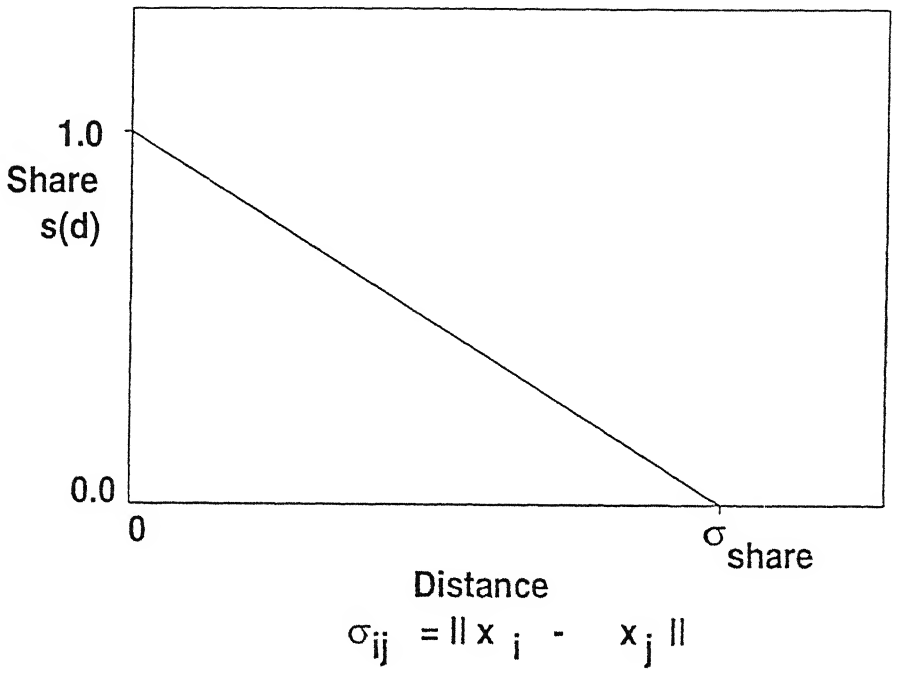

Figure 2.2: Triangular sharing function (Source: [19])

for all the strings. This distance is generally taken in a normalized form. Thus for any string its share is obtained by summing up all the differences for the niched parameters. Eventually for a given string the total extent of sharing is determined by summing up the contribution of each individuals in the entire population. Thus any individual in proximity with the given string has a sharing function value close to one; the further away the string is, the sharing function value decreases correspondingly. On getting the total sharing function value the individuals fitness is degraded using the following scheme

$$f_s(x_i) = \frac{f(x_i)}{\sum_{j=1}^{n} s(d(x_i, x_j))} \tag{2.19}$$

2.5 MicroGA

The simple genetic algorithm (SGA) discussed above uses only three basic GA operators, namely reproduction, crossover and mutation. This kind of GA is suitable for stationary function optimizations, but fails to optimize non-stationary functions where the function itself is evolving at a rate faster than SGA's [26]. This kind of real-world problems include problems in aerospace, such as pursuit and evasion, on-line aircraft trajectory optimization, optimal control of aircraft in wind shear [26] etc. Krishnakumar [26] proposed a new scheme of genetic algorithm for application in such purposes and also in stationary optimization. The stepwise procedure for microGA implementation as proposed by [26] is given below

1. A micro-population usually of size 5 is selected randomly including one good string from the previously conducted search.

2. The individual fitnesses are evaluated and the best string is identified. The best individual is then passed into the next generation (elitist strategy). This procedure guarantees the preservation of good schema.

3.The remaining four strings are chosen using a tournament selection strategy. Here a deterministic tournament selection method [19] is used since the law of averages does not hold good for small population sizes as used in microGA. Simultaneously precautions should be taken to prevent mating of same strings for the next generation.

4.Crossover is then applied on the selected individuals. A crossover rate of $p_c = 1$ is to be used. This implies that each and every string is subjected to crossover action. Using a high crossover rate is expected to promote schema processing; the mutation rate is kept at zero as enough diversity is introduced into the population through the crossover action.

5. The population is then checked for convergence (either genotypic or phenotypic convergence). If convergence is achieved we then proceed to step 1.

6. Else to step 2.

2.6 Inversion

In nature the functionality of a chromosome is independent of its gene positions. This is however not the case in genetic algorithm, where bit positions comes to play an important role. For enabling GA's to mimic nature the inversion operator was developed. Here each gene in a chromosome is attached to an identifier giving the locus of that gene. Hence the identity of a chromosome can be preserved independent of the position of its genes. Thus in ordinary binary GA a four bit string 1101 is stored under inversion conditions as (1,1), (1,2), (0,3), (1,4). Under such a situation the position of a gene is no longer necessary to be fixed. The inversion operator in genetic algorithm is implemented by fixing two bit positions on the chromosome randomly and then reversing the sequence of genes in between these two positions. Thus consider that the two bit positions selected for the 4-bit string shown above are situated in between the first and second and second and third bit positions respectively. After inversion the new string is given as (1,1), (0,3), (1,2), (1,4). The genetic operators of crossover and mutation are then allowed to operate on this string. It may be noted that the normal crossover operator under inversion conditions is redundant since this would entail the possibility of same genes being repeated in the new chromosome. Thus starting with two strings (1,1), (0,3), (1,2), (1,4) and (1,0), (1,2), (0,3), (1,4) with the crossover point chosen in between the 2^{nd} and 3^{rd} bit positions crossover yields two offsprings (1,1), (0,3), (0,3), (1,4) and (1,0), (1,2), (1,2), (1,4). Thus the same genes gets repeated in the chromosome making the crossover redundant. To avoid this situation certain strategies have been proposed [19, 22]. One of the strategy is to allow crossover between strings which have homologous loci for its genes [19]. This evidently imposes a strict restriction limiting the availability of strings suitable for crossover. A second strategy proposed is to consider one of the parent string as the "master string" [22] and the other as "slave". Before crossover the slave string genes are arranged in the same combination of the master string. The original combination of slave string is restored after the crossover operator is executed. Evaluation

of the fitness of new string evolved is then done by arranging the strings according to their locus.

2.7 Differential Evolution

Besides genetic algorithm a newer evolution technique has also been used as an optimization tool for obtaining the ground state structures of a-Si:H clusters. This method known as Differential evolution has been described by Kenneth Price and Rainer Storn [27]. In simple GA strings or the chromosomes (speaking biologically) are our starting material requiring a binary encoding. In DE the concept is different in the sense that real valued vectors are taken as the starting population and vector differentials instead of genetic differences is the driving force behind fitness improvement. An individual in DE thus comprises of an array of variables represented in real numbers. Starting with a random population the *cost functions* of the individuals are first evaluated. This step is followed by mutation, crossover and selection which are redefined in the present context. Any vector in the initial array is chosen as the parent. Two individuals are then randomly picked up from the given population with care taken to prevent selecting the same string twice. The difference between these two vectors are then calculated (see Fig. 2.3). Thus consider $\vec{X}$ and $\vec{X}_i$ are the two selected vectors whose difference is given as $(\vec{X} - \vec{X}_i)$. This *difference vector* is then multiplied with a parameter, known as *DE mutation constant* (F). The weighted difference vector thus created is added to a third vector $\vec{X}_j$ chosen randomly from the population forming another parent, which is given as

$$\vec{X}_{new} = \vec{X}_j + F.(\vec{X} - \vec{X}_i) \tag{2.20}$$

Crossover is then performed between vectors $\vec{X}_{new}$ and the parent creating the *trial vector*. The mechanism of crossover involves substituting the variable in the parent with that of

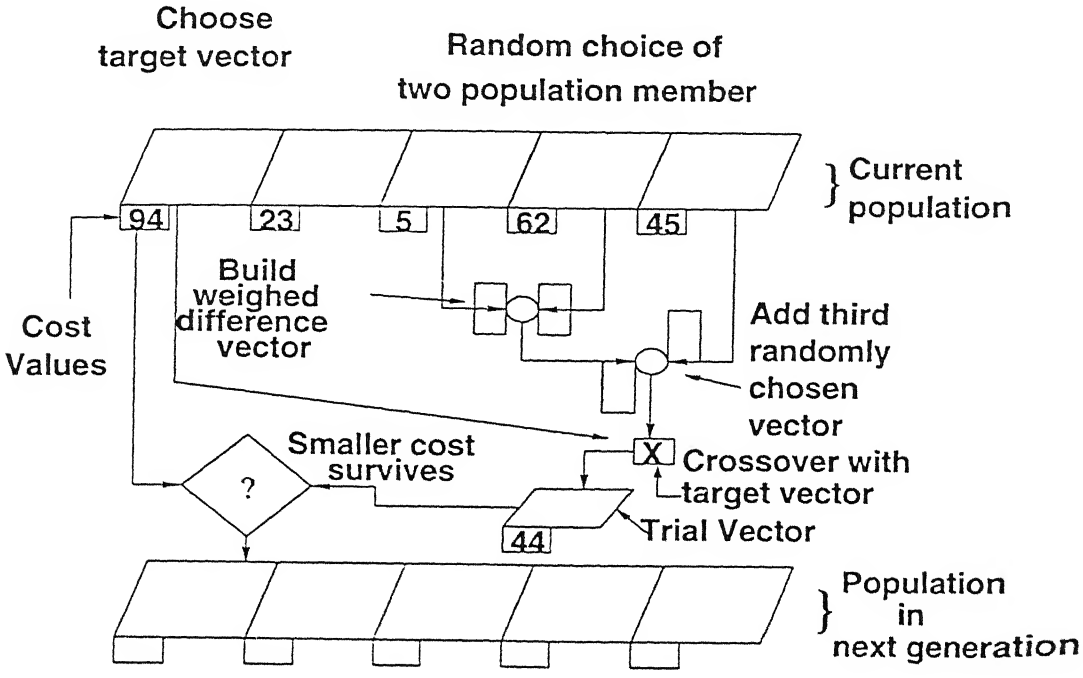

Figure 2.3: Basic mechanism of differential evolution (Source: [27])

$\vec{X}_{new}$ on the basis of some probability. A uniform random number is generated, which if greater than the crossover probability triggers variable swapping. This process is done by selecting the variables on a random basis obtained by performing a series of D-1 binomial experiments [2]. To ensure diversity in the population the last component to be changed is always taken from $\vec{X}_{new}$. The trial vector thus evolved is then evaluated for its cost value. If the cost value is lesser than that of parent vector it is accepted into the next generation. This process is performed N times (N being the population size), each vector being selected once to play its role as a parent. Depending upon the problem to be optimized, the strategy for trial vector creation can be suitably changed. Further information in this regard is available in [27].

[2]For further elaborations see [27]

Chapter 3

Problem Formulation

Molecular structure optimization involves finding out the configuration for which total energy is minimum. Such a structure is energetically most stable and corresponds to the ground state structure. In order to achieve this through self-consistent calculations, the density functional theory (DFT) by Kohn and Sham [28] can be used, which however involves very large-scale computations. To avoid this computational overhead, efforts were made to calculate the total energy of clusters using semi-empirical models. Non-orthogonal tight binding theory is one of the commonly used model for simulating semiconductor systems like silicon. Here the total energy of the system is taken as :

$$E^{total}(\mathbf{R}) = E^{pair} + E^{el} + U_0 \tag{3.1}$$

Where E^{pair} denotes the summation of repulsive pair potential terms χ_{ij} for the cluster and is given as:

$$E^{pair} = \sum_{i=2}^{N^{atom}} \sum_{j=1}^{i-1} \chi_{ij} \tag{3.2}$$

The electronic energy (E^{el}) is given by the expression

$$E^{el} = \sum_{k=1}^{N^{elec}} g_k.\epsilon_k \tag{3.3}$$

where g_k is the occupancy of the k'th eigenvalue ϵ_k. Further details regarding the calculation of ϵ_k and χ_{ij} are discussed in Sections 3.1 and 3.2. The correction factor U_0 comprises of U_0^{Si} and U_0^H contributions for each of the atoms of silicon and hydrogen which is further described in Section 3.2.

3.1 Calculation of the Eigenvalues

According to the non-orthogonal tight binding theory the eigenvalue problem can be expressed as

$$H|\psi_k\rangle = \epsilon_i|\psi_k\rangle \tag{3.4}$$

Unlike in DFT the Hamiltonian in non-orthogonal tight binding theory (NOTBT) is not evaluated from the first principles. They are obtained by using a model chosen on the basis of its ability to simulate the system. The eigenfunctions are then expressed in terms of a suitable basis set. Thus considering that $|\phi^i\rangle$ denotes the i'th function of the basis set the i'th eigenfunction can then be written as

$$|\psi_k\rangle = \sum_k C_k^l|\phi_k\rangle \tag{3.5}$$

It is implicitly assumed here that, the basis set $|\phi^i\rangle$ chosen is sufficiently large and accurately represents the eigenfunctions of the system. The eigenvalue problem can thus be represented as

$$H\sum_m C_n^m|\phi^m\rangle = \epsilon_n\sum_m C_n^m|\phi^m\rangle \tag{3.6}$$

Multiplying the above equation with $\langle\phi^i|$ we get

$$\sum_m \langle\phi^l|H|\phi^m\rangle = \epsilon_n \sum_m C_n^m \langle\phi^l\|\phi^m\rangle \tag{3.7}$$

On defining the matrix elements H_{lm} and S_{lm} as

$$H_{lm} = \langle\phi^l \mid H \mid \phi^m\rangle \tag{3.8}$$

$$S_{lm} = \langle\phi^l\|\phi^m\rangle \tag{3.9}$$

the characteristic equation obtained is

$$\sum_m (H_{lm} - \epsilon_n S_{lm}) C_n^m = 0 \tag{3.10}$$

The above equation is solved for the eigenvalues using standard numerical techniques.

3.2 Determination of Model Parameters

Silicon atom consists of one s and three p orbitals while hydrogen has one s orbital. Depending upon the type of orbitals and the nature of their overlap, four Hamiltonian matrix elements, $H_{ss\sigma}$, $H_{sp\sigma}$, $H_{pp\sigma}$, $H_{pp\pi}$ and four overlap integrals $S_{ss\sigma}$, $S_{sp\sigma}$, $S_{pp\sigma}$, $S_{pp\pi}$ are defined. The matrix elements in non-orthogonal theory are taken according to [29]. If V_{ij} denotes the Hamiltonian matrix elements in the orthogonal theory then H_{ij} is given by,

$$H_{ij} = V_{ij}[1 + \frac{1}{\kappa} - S_2^2] \tag{3.11}$$

If both atoms have s and p orbitals (e.g: matrix elements between two silicon atoms) then S_2 is given as

$$S_2 = \frac{S_{ss\sigma} - 2\sqrt{3}S_{ss\sigma} - 3S_{ss\sigma} + 3S_{pp\pi}}{4} \tag{3.12}$$

For one atom having s orbital and the other both s and p orbitals (e.g: matrix elements for a Si and H atoms) S_2 is given by

$$S_2 = \frac{S_{ss\sigma} - \sqrt{3}S_{sp\sigma}}{2} \tag{3.13}$$

When both atoms have s orbitals only (e.g: for two hydrogen atoms), S_2 is given by

$$S_2 = S_{ss\sigma} \tag{3.14}$$

The overlap integrals $S_{ss\sigma}$, $S_{sp\sigma}$, $S_{pp\sigma}$ and $S_{pp\pi}$ are given as

$$S_{\lambda\lambda'\mu} = \frac{2V_{\lambda\lambda'\mu}}{\kappa(\epsilon_\lambda + \epsilon_{\lambda'})} \tag{3.15}$$

where $V_{\lambda\lambda'\mu}$ are the Hamiltonian matrix integrals in the orthogonal theory, κ the non-orthogonality coefficient-efficient and ϵ_λ, $\epsilon_{\lambda'}$ are the Hamiltonian matrix elements for the λ and λ' orbitals respectively.

In this work, Hamiltonian matrix integrals of the orthogonal theory are assumed to have the form

$$V_{\lambda\lambda'\mu}(r_{ij}) = V_{\lambda\lambda'\mu}(d_0)exp\{-\alpha(r_{ij} - d_0)\} \tag{3.16}$$

where r_{ij} is the distance between atoms and d_0 the bond length parameter. The repulsive pair-potential term is expressed in the form :

$$\chi(r_{ij}) = \chi_0 exp[-4\alpha(r_{ij} - d_0)] \tag{3.17}$$

The non-orthogonality coefficient-efficient κ is given as

$$\kappa(r_{ij}) = \kappa_0 + \alpha(r_{ij} - d_0)^2 \tag{3.18}$$

where κ_0 and α depends on the nature of atoms considered. The Hamiltonian matrix elements for the λ orbital ϵ_λ, depends only on the type of atom considered. Additional restrictions were imposed on the H-H interaction in the form of a cut-off function given as [18]

$$f_{\text{cut}}(r_{ij}) = \frac{1}{1 + exp[\frac{r_{ij} - r_{cut}}{s_{cut}}]} \tag{3.19}$$

The off-diagonal terms in the Hamiltonian and H-H pair potentials were multiplied by this function [18]. Further justifications for this can be found in [18].

For silicon the Hamiltonian matrix elements ϵ_s^{Si}, ϵ_p^{Si} the bond-length parameter d_0^{Si-Si}, $V_{ss\sigma}^{Si-Si}$, $V_{sp\sigma}^{Si-Si}$, $V_{pp\sigma}^{Si-Si}$, and $V_{pp\pi}^{Si-Si}$ were obtained from the work of Harrison [30] while the parameters α^{Si-Si}, κ_0^{Si-Si}, and ψ_0^{Si-Si} are from the work of Menon and Subbaswamy [31]. The correction factor C_0^{Si} for silicon has also been adapted from [31].

Parameters for Si-H interactions were obtained by fitting the experimental values of bond length, cohesive energy and vibration frequencies (A and E mode) for silane through least squares method [18]. This includes the parameters ϵ_s^H, U_0^H, d_0^{Si-H}, $V_{ss\sigma}^{Si-H}$, $V_{sp\sigma}^{Si-H}$, α^{Si-H}, κ_0^{Si-H} and χ_0^{Si-H}. The H-H interaction parameters were obtained in a similar fashion using the experimental data on hydrogen molecule [18]. Parameters values used for each of the interactions are given in Tables 3.1 - 3.2. It is worth mentioning here that, the last term U_0 in the total energy term is a correction factor, whose contribution in effect is taken as a constant throughout our calculation for the cluster.

Table 3.1: Interaction parameters for Si-Si, Si-H and H-H

Parameters	Si-Si	Si-H	H-H
d_0(Å)	2.36 [30]	1.48 [18]	0.74 [18]
χ_0 (ev)	0.05 [30]	2.4365 [18]	2.674 [18]
κ_0	1.70 [31]	5.90 [18]	3.30 [18]
α (Å^{-1})	1.60 [31]	0.7563 [18]	1.200 [18]
$V_{ss\sigma}$ (ev)	-2.37 [30]	-4.02 [18]	-13.250 [18]
$V_{sp\sigma}$ (ev)	2.52 [30]	5.52 [18]	-
$V_{pp\sigma}$ (ev)	3.32 [30]	-	-
$V_{pp\pi}$ (ev)	-1.07 [30]	-	-
r_{cut} (Å)	-	-	1.57 [18]
s_{cut} (Å)	-	-	0.05 [18]

Table 3.2: Parameters for Si and H atoms

	ϵ_s (ev)	ϵ_p (ev)	U_0 (ev)
Si	-13.55 [30]	-6.52 [30]	1.000 [31]
H	-10.77 [18]	-	4.721 [18]

3.3 Application of GA

Considering an atom to be a sphere with its mass concentrated at the center, any molecular structure is completely specified by the coordinates of the centers of its constituent atoms. In this work a cluster was considered to be situated within a cubic search space described by a Cartesian coordinate system. Thus in a cluster of type Si_nH_m, a total of m+n atoms can be explicitly described in terms of 3(m+n) coordinates. These 3(m+n) variables are mapped onto their corresponding binary forms, which on being assembled together gives rise to an individual ready for further genetic processing. Thus consider the following individual

100101011101011

which represents the position of an atom in a cubic box of 125 cubic Åvolume. The x, y, and z coordinates are represented by the 5 bit sub strings 10010, 10111 and 01011 respectively. Decoding the x, y, z sub strings into their real values using Eqn. 2.2, we get

$$x = 2.90 \text{ Å}$$
$$y = 3.71 \text{ Å}$$
$$z = 1.77 \text{ Å}$$

An individual is then checked for constraint violations prior to any further processing. The constraints imposed on a structure involve the minimum distances that must be maintained between Si-Si, Si-H and H-H atoms to prevent the atoms in the cluster from collapsing onto itself. Individual bond length parameters in Table 3.1 were generally used as the guideline. Attributing a low fitness value to an individual, which effectively rules out its transfer to the next generation, properly penalizes any violation of these constraints. Structures satisfying all these constraints are evaluated for their cohesive energy, the negative of which is assigned as the fitness. Ours being a minimization problem, an individual with the lowest cohesive energy receives the highest fitness value.

Initially creating a random population generates a set of random structures whose individual fitness values are evaluated. Then the genetic operators discussed earlier are applied to this population giving birth to the individuals of the next generation. This process is continued till the population evolves to produce the fittest individual, which is then decoded to get the ground state structure.

Chapter 4

Computational Details

4.1 Genetic Algorithm

As discussed previously in Chapter 2, the search space in this problem consists of a cube. For all the calculations reported in this work, the side of cube was taken between 4 to 7 Å. The string length for each variable was chosen such that the minimum resolvable distance remained around 0.01 Å, or less. Thus for each variable, a 10-bit string was chosen at the least. Population size was kept in the range 90 - 100. Initially all the strings were niched for each of the variables using Goldberg's triangular sharing function [19]. The objective was to prevent premature convergence and maintain an uniform selection pressure throughout the calculation as indicated earlier. This was followed by the application of reproduction operator. Tournament selection of size two coupled with elitist strategy was utilized for this purpose. The reproduction process was proceeded by the single point crossover operation. A crossover probability of 0.78 was generally used. Alternately, for bigger clusters (i.e for Si_7H and Si_8H) two-point crossover was also applied with crossover probability in the range 0.85 - 0.95.

Crossover was followed by the mutation operation. Both jump and creep mutation operators were exercised. Jump mutation probability was chosen in the range of 0.01 and

less. In all problems, the probability value for creep mutation was initially kept at 0.0011 which was increased at higher generations. Depending upon the population variance at higher time steps, jump mutation probability was also adjusted to retain genetic diversity. For clusters in the series Si_mH_n, total number of function evaluations required increases with the cluster size to be optimized. The overall strategy for optimization consisted of invoking runs from different initial conditions with the best result among all the runs being considered as the required global optimum. The stopping criteria for a run was kept at 1,00,000 function evaluations.

For clusters SiH, SiH_2, SiH_3, Si_2H, Si_2H_2, Si_2H_3, Si_2H_4, Si_3H and Si_4H, ground state results were obtained in less than 12,000 function evaluations. The optimum cohesive energy for clusters SiH_4 and Si_2H_5 were deduced within 30,000 function evaluations. For clusters Si_5H, Si_6H and Si_7H, a steep rise in the number of function evaluations were registered. Comparable results to simulated annealing [38] were achieved after approximately 70,000 function evaluations. The Si_8H cluster posed the maximum difficulty with required function evaluations exceeding 1,00,000. This also indicates a non-linear increment in problem stiffness with increasing problem dimension.

4.2 Differential Evolution

Some of the clusters were also optimized using differential evolution algorithm. In this method the search space considered was identical to that used in GA. Initially an assortment of random vectors was considered. The population used was generally in the range 90 - 100. At the beginning of the search process, a high crossover rate (0.8 - 0.9) was applied in accordance with the suggestion of Price and Storn [27]. This was followed by runs using a crossover probability in the range 0.5 - 0.6 with the F value varying between 0.6 - 0.7. As population converged, the crossover probability was reduced to a still lower magnitude of about 0.2 with a simultaneous decrease in the F value. The search process was continued

till the given stopping criteria was satisfied.

All calculations in this work were done using a public domain FORTRAN 77 code [32] with several modifications. The suitability of the code had been previously confirmed in a separate study [33]. The entire computational job was performed in the local area network (LAN) at Indian Institute of Technology Kanpur, predominantly using a Silicon Graphics server with central processing units : MIPS R10000, Rev 2.6 under IRIX64 Release6.4 operating system. The graphics output of the cluster geometries were generated using the XMol software on a SUN Solaris workstation.

Chapter 5

Results and Discussion

Cohesive energies of the different ground state structures are given in Table 5.1 below. This table also provides a comparison with the previously published data in literature.

Table 5.1: Ground state energy of various Si-H clusters

Cluster	Present Study (-ev)	Simulated Annealing [18, 38] (-ev)
SiH	2.97	2.97
SiH_2	7.037	7.04
SiH_3	8.90	8.90
SiH_4	13.409	13.41
Si_2H	6.56	6.57
Si_2H_2	10.139	10.14
Si_2H_3	12.86	12.87
Si_2H_4	17.008	16.93
Si_2H_5	17.907	17.51
Si_3H	10.598	10.624
Si_4H	14.82	14.83
Si_5H	19.385	19.42
Si_6H	23.895	23.90
Si_7H	28.139	28.147
Si_8H	32.443	32.445

The bond lengths and bond angles of clusters are provided in Tables B.1 - B.14. Struc-

tures obtained in this study are discussed in the following sections. In the figures given below the Si-H distances greater than 1.6 Å but less than 2.0 Å are shown in dark shades, while those still lesser are unshaded. Similarly for denoting Si-Si distance greater than 2.5 Å and less than 3 Å, dashed line has been used. The above choices are based upon the accepted covalent distances for these atom combinations.

5.1 SiH_2

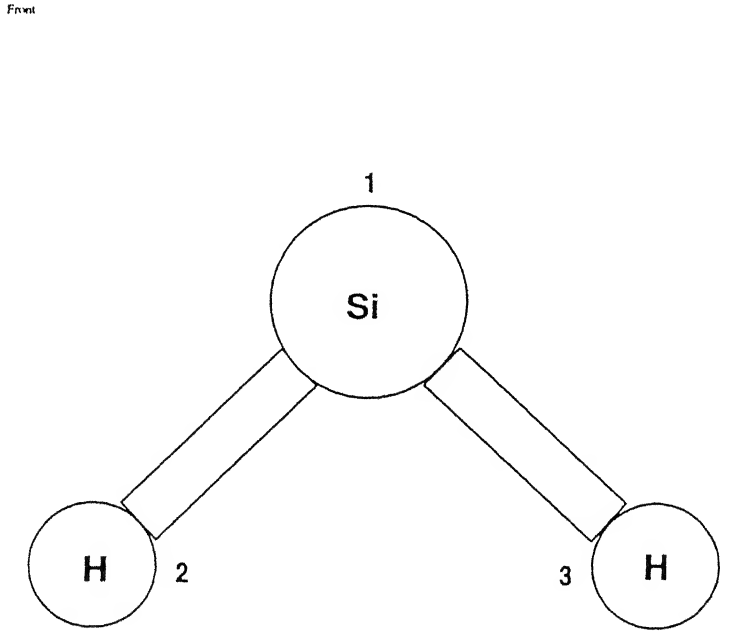

Figure 5.1: Ground state configuration of SiH_2

SiH_2 exhibits a planar symmetrical structure. In this work the distance between the Si-H atoms is calculated as 1.51 Å, and the ∠H-Si-H is found to be 89.97°. These values are in agreement with the experimental values of 1.5141 Å, and 92° [34, 35] and the optimized results of simulated annealing [18].

5.2 SiH_3

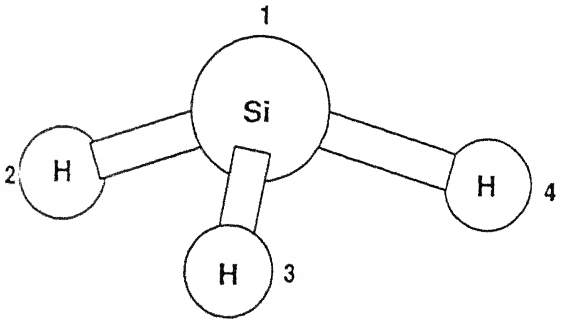

Figure 5.2: Ground state configuration of SiH_3

SiH_3 possesses a pyramidal structure. The distance between silicon and hydrogen resembles that for a covalent bonding with a bond length of ~ 1.5 Å. The ∠H-Si-H is approximately around 107° .

5.3 SiH_4

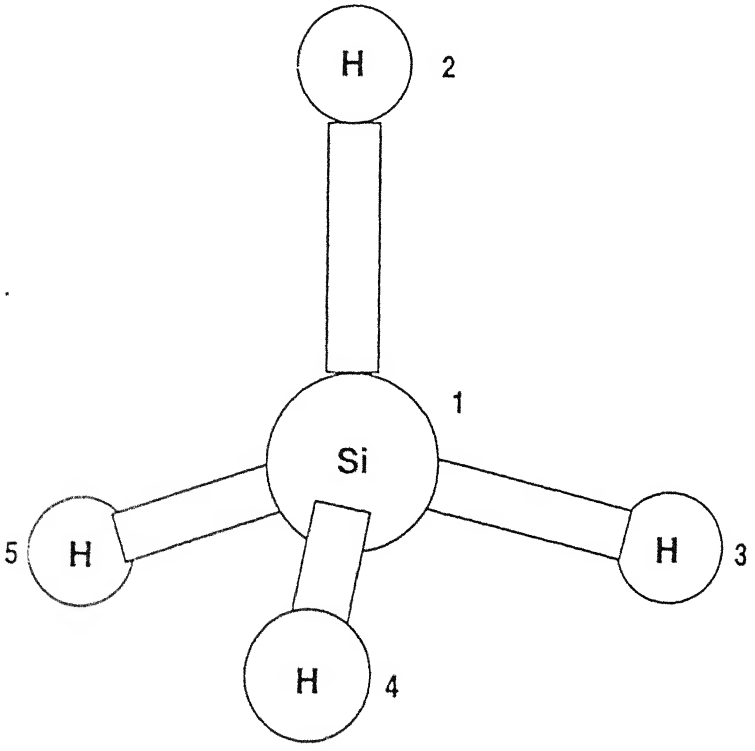

Figure 5.3: Ground state configuration of SiH_4

SiH_4 has a tetrahedral structure. The optimized structure matches well with the structure obtained experimentally [36]. This revalidates the parameters chosen for the purpose of our cohesive energy calculation. Distance between the Si-H atoms is obtained as 1.48 Å, and the calculated ∠H-Si-H varies from 106.4 to 111.6°. The cohesive energy values are well in accord with the results of [18] and [37].

5.4 Si_2H

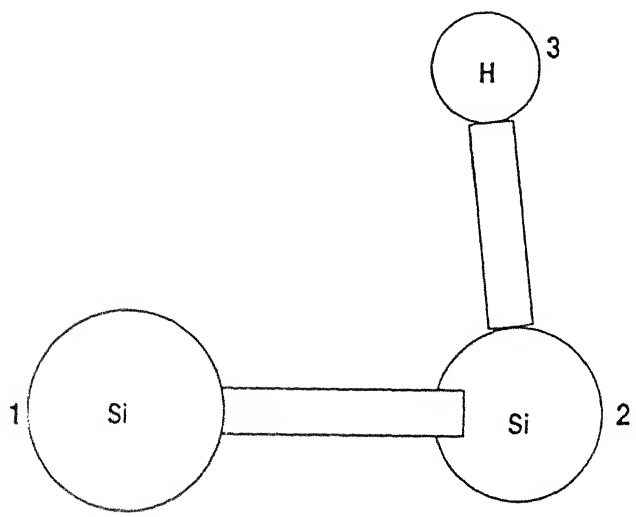

Figure 5.4: Ground state configuration of Si_2H

Si_2H exhibits a non-symmetrical structure. Si-Si distance is obtained as 2.34 Å. The lone hydrogen atom is bonded strongly with one of the silicon atom, being situated at a distance of 1.54 Å, which is similar to that obtained for covalent bonding. This structure is equivalent to the structure obtained by [18].

5.5 Si_2H_2

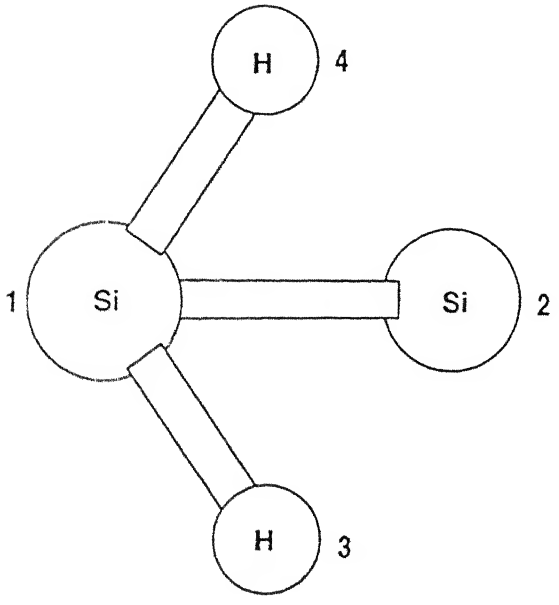

Figure 5.5: Ground state configuration of Si_2H_2

In Si_2H_2, the two silicon atoms are bound to each other with their bond lengths comparable to that found in Si_2H. Both hydrogen atoms are bonded strongly to one of the silicon atoms with a bonding distance of approximately 1.54 Å, and are oriented as mirror image to each other. The structure obtained is in agreement with the results of [18].

5.6 Si_2H_3

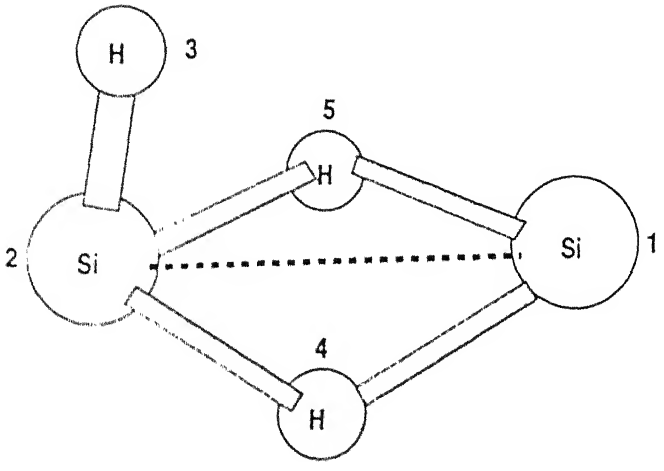

Figure 5.6: Ground state configuration of Si_2H_3

The Si_2H_3 structure determined in this study shows that the bond length between its two Si atoms is greater than the accepted value for covalent bonding. This structure differs from Si_2H_2 and Si_2H, both in the Si-Si bond length and also in the arrangement of hydrogen atoms. Hydrogen atoms 4 and 5 are situated symmetrically with respect to silicon atoms 1 and 2. The third hydrogen atom is placed nearer to silicon atom 1 with the bond distance resembling that of Si-H covalent bond. This structure closely resembles the

simulated annealing result of [18].

5.7 Si_2H_4

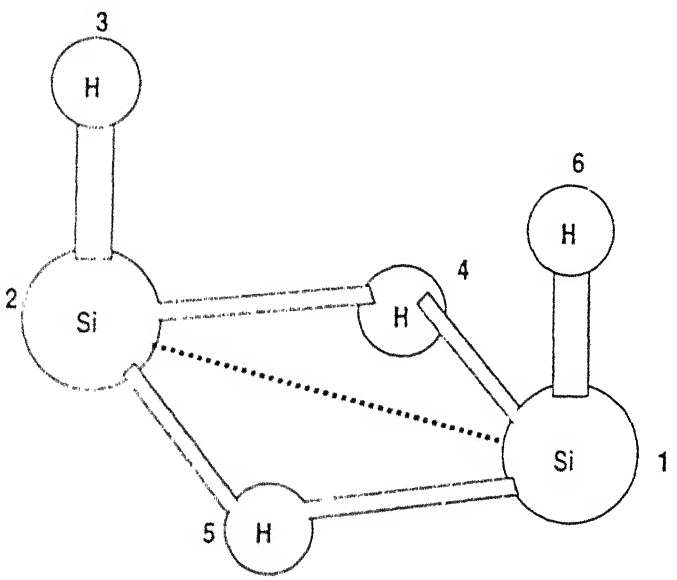

Figure 5.7: Ground state configuration of Si_2H_4

Structure of Si_2H_4 calculated in the present work is however, in variance with the simulated annealing results of [18]. The Si-Si distance and the arrangement of hydrogen atoms closely resemble to those in Si_2H_3. While two hydrogen atoms are situated in symmetry with the silicon atoms, at a distance more than 1.7 Å, the other two atoms are attached

to one silicon atom each; their distance being approximately 1.5 Å. Both of these hydrogen atoms are oriented on the same side, unlike the structure reported by [18].

5.8 Si_2H_5

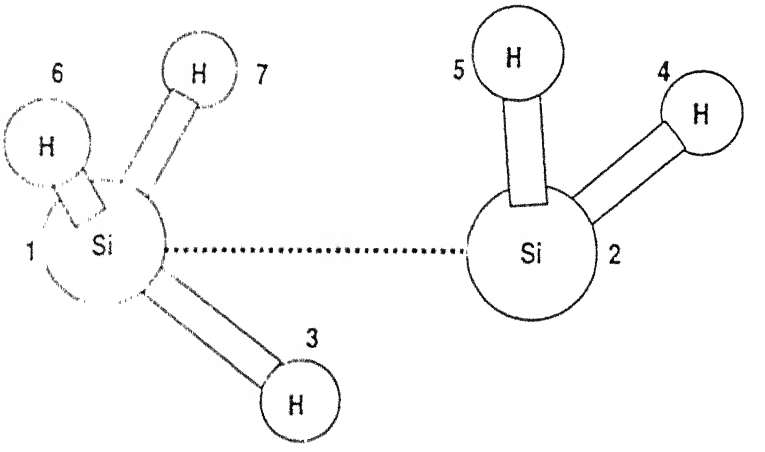

Figure 5.8: Ground state configuration of Si_2H_5

The cohesive energy obtained for Si_2H_5 is -17.907 ev which is lower compared to -17.51 ev obtained [18]. The Si-Si bond length obtained is 2.995 Å, compared to 2.29 Å, reported

in the simulated annealing studies. Three hydrogen atoms are situated closely to one silicon atom, while the remaining two are attached to the other silicon. The Si-H bond length in each of these instances is quite alike the accepted Si-H covalent bond length.

5.9 Si_3H

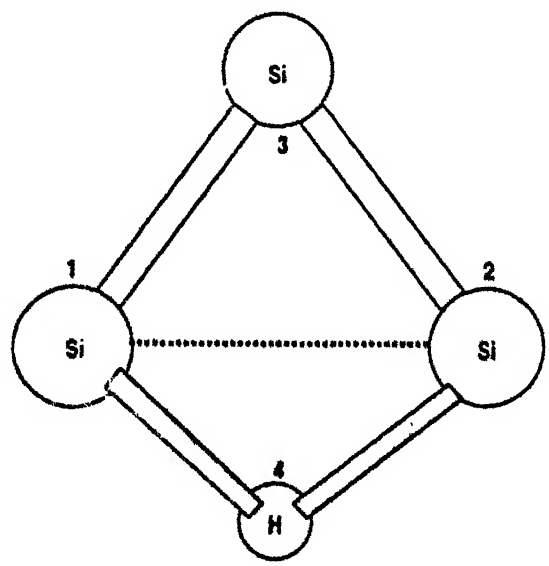

Figure 5.9: Ground state configuration of Si_3H

In the Si_3H structure silicon atoms 1 and 2 are situated symmetrically with respect to the third. The lone hydrogen atom is situated equidistantly from Si atoms 1 and 2. The Si-H bond distance being of the order of 1.8 Å, which is greater than that existing in SiH cluster. Gupte and Prasad [18] studied the characteristic frequency of the Si-H bond and

found its highest vibrational frequency to be 1378 cm^{-1}. This indicates that the Si-H bond in this cluster is weak.

5.10 Si_4H

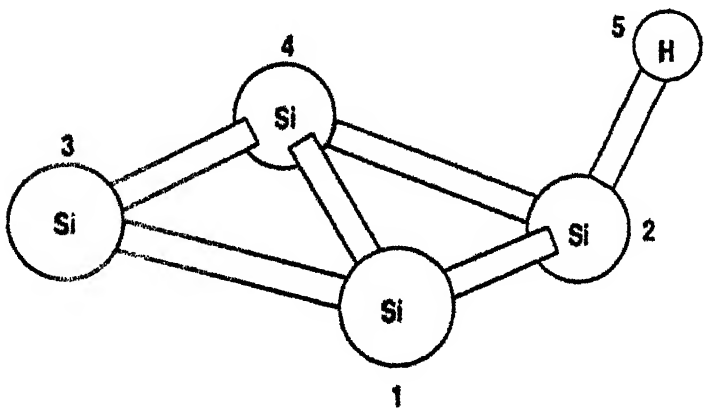

Figure 5.10: Ground state configuration of Si_4H

The ground state structure of Si_4H is quite similar to that of Si_4 cluster [31]. The existence of hydrogen atom has only caused some distortion in the structure, retaining the essential geometrical feature of Si_4. The hydrogen atom is situated at a distance of 1.54 Å,

from the silicon atom 2 which is quite alike that existing in Si-H covalent bond. Vibrational frequency study of the Si-H bond by [38] indicates the highest frequency as 2200 cm^{-1}, which proves the presence of a strong Si-H bond for this system.

5.11 Si_5H

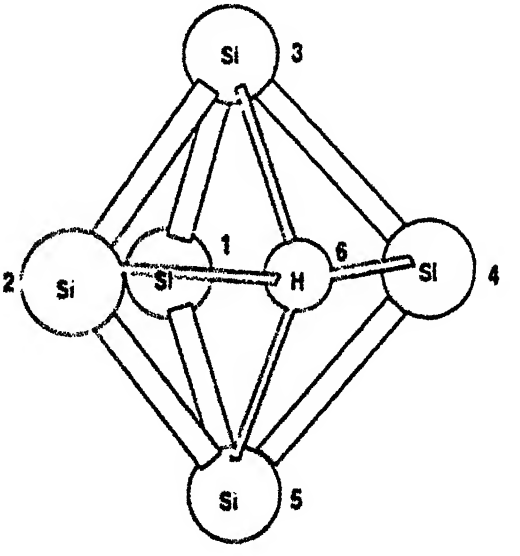

Figure 5.11: Ground state configuration of Si_5H

Si_5H ground state structure as shown in the figure shows that the hydrogen atom is lying in the same plane as that of silicon atoms 1,2 and 4. The hydrogen atom is situated closer to the silicon atoms 1 and 2 with Si-H distance being around 1.84 Å. Vibrational spectrum studies [38] also indicate the absence of the characteristic frequency of strong Si-

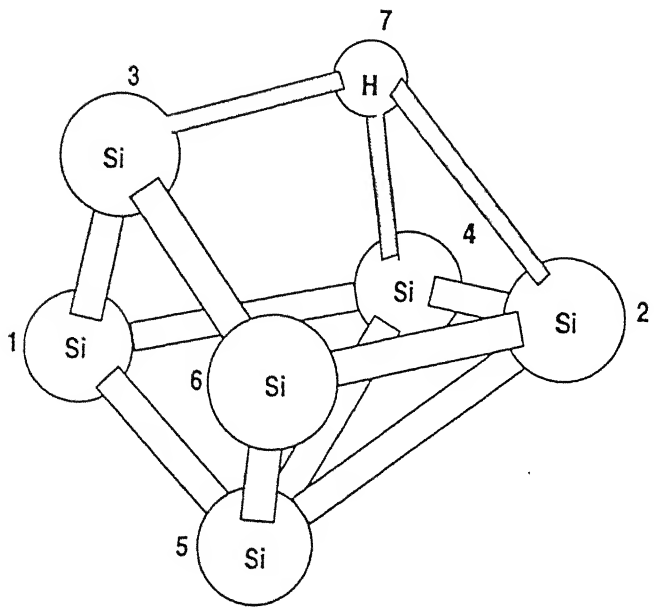

Figure 5.12: Ground state configuration of Si_6H

H bond (2100 cm^{-1}). The ground state structure is quite different from that found using simulated annealing [38]. It is evident that our results are a manifestation of a metastable state the cohesive energy being 0.03 ev higher than that found by simulated annealing.

5.12 Si_6H

The structure of Si_6H obtained in this work is similar to the results of simulated annealing [38] and shows a remote correlation with the Si_6 configuration reported [39].

Raghavachari and Rohlfing [39] have suggested two alternate structures for Si_6 consisting of either an edge-capped trigonal bipyramid or a bicapped tetrahedron geometry. The structure of Si_6H appears to be a grossly distorted bicapped tetrahedron, hydrogen causing the nodal silicon atom 3 to be displaced from its centered position in Si_6. The optimized structure obtained through GA is 0.0046 ev more energetic than that of simulated annealing. This energy difference is manifested in the variation of Si-H bond distances (± 5%). The maximum variation exists for the distance between atom numbers 2 and 7 with bond lengths differing by 0.10 Å. However the Si-Si bond distances obtained are nearly same with the differences being less than ± 1% while the angular measures vary within ± 5 %.

5.13 Si_7H

The optimized geometry for Si_7H predicted through GA differs from the results of simulated annealing [38] being 771 Joules/mole less stable. Thus the result of GA indicates the existence of a metastable geometry for this cluster. The structure obtained however possesses a gross similarity with the capped trigonal prism structure for Si_7 (C_{2v} symmetry) considered by Raghavachari and Rohlfing [39]. For the Si_7 structure thus proposed, the silicon atom 7 is arranged in a pyramidal fashion with atoms 1, 3, 5 and 6 constituting its basal plane (see Fig. 5.13(a)). The introduction of a hydrogen atom causes the atom 7 to shift towards one edge of the pyramid base. Comparing the ground state structure of Si_7H [38] to that of Si_7 (pentagonal bipyramid with D_{2h} symmetry) [31, 39], the hydrogen atom is found to position itself between silicon atom 7 and the mid plane comprising of 5 silicon atoms (see Fig. 5.13(b)). It is to be noted that the optimized structure presented in this work differs radically from the proposed ground state structure for Si_7H [38] in the absence of penta-bonded silicon atoms.

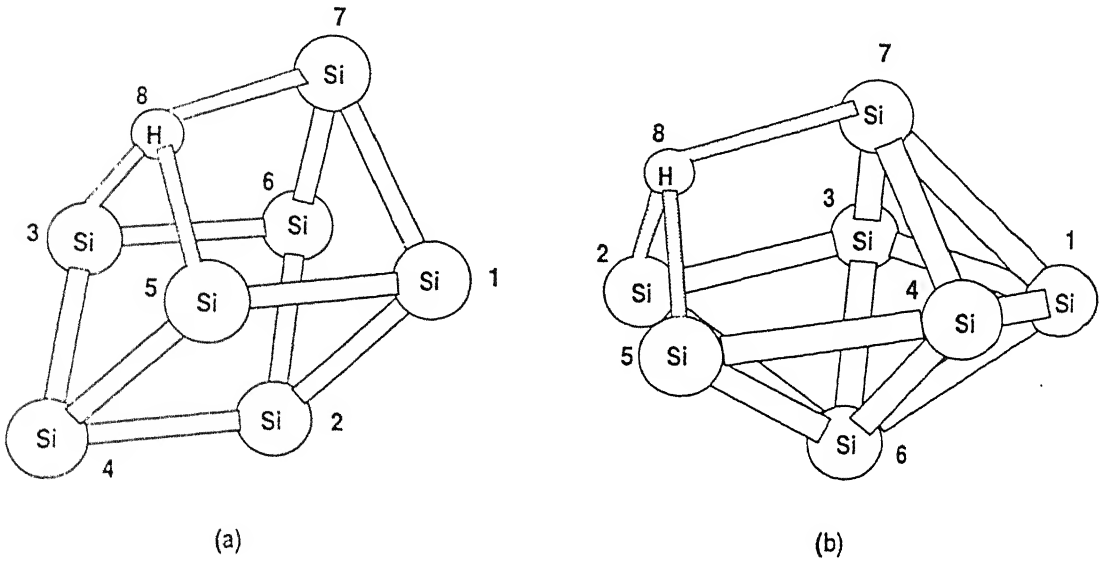

Figure 5.13: (a) Metastable configuration of Si_7H obtained through GA (b) Ground State configuration of Si_7H obtained through simulated annealing (Source: [38])

5.14 Si_8H

Ground state configuration for Si_8H obtained through GA, conforms with the simulated annealing results [38] with a cohesive energy difference of 0.0018 ev. The optimized structure is approximately similar to that of Si_8. Menon and Subbaswamy [31] has proposed a distorted bicapped octahedron structure as the lowest energy state for Si_8. The addition of a hydrogen atom modifies this geometry further. Thus the H atom seems to push silicon atoms 6 and 8 (see Fig. 5.14) further apart, compared to their positions in Si_8. The hydrogen atom thereby, lies nearest to atoms 6 and 8 at a distance of $\sim$ 1.75 Å which is much greater than the accepted covalent distance for Si-H. The next nearest neighbors i.e., atoms 1, 2, 3 and 4

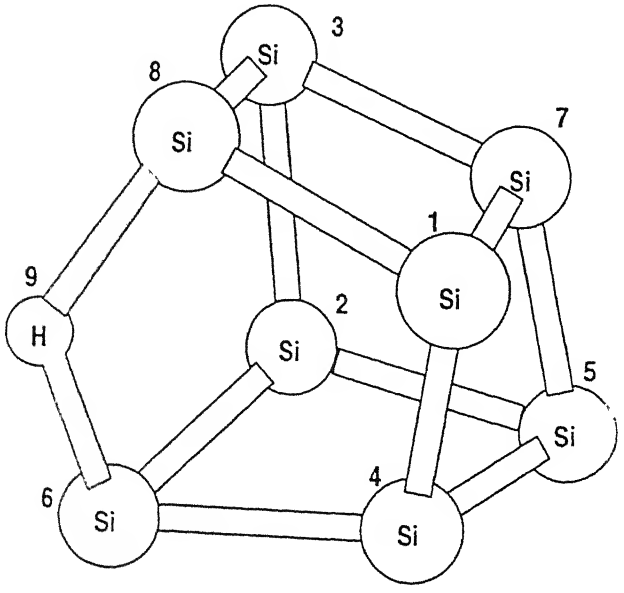

Figure 5.14: Ground state configuration of Si_5H

are placed at a distance of ~ 3.0 Å.

5.15 Results of DE

Differential evolution (see section 2.7) method has been used an alternate evolutionary optimization technique in this work. Initially the smaller clusters of Si_mH_n series have been optimized as a test case. The cohesive energies of clusters thus obtained, are listed in Table 5.2. Preliminary results are comparable to those of GA. Further work with this approach is

required to establish the relative advantages or disadvantages of DE over GA.

Table 5.2: Results of Differential Evolution

Cluster	Results of DE(ev)	Results of GA(ev)
Si_2H	6.56	6.57
Si_2H_2	10.09	10.139
Si_2H_3	12.85	12.87
SiH_2	7.04	7.04
SiH_3	8.90	8.90

Chapter 6

Conclusions

Ground state structures of Si_nH_m clusters for (n= 1,2 and m= 1,5) and Si_lH clusters for (l=3,8) have been optimized using a tight binding non-orthogonal scheme coupled with genetic algorithm. Most of the results obtained in this study compare well with those obtained from available experimental work and the optimized results of simulated annealing [18, 38]. The structures obtained for Si_2H_4, Si_2H_5, Si_5H and Si_7H are the only ones, which significantly differ from the work of Gupte and Prasad [18, 38]. The cohesive energy values determined for Si_2H_4 and Si_2H_5 are lower than those obtained through simulated annealing, rendering the structures reported in this work thermodynamically more favorable. Using a similar line of reasoning, structures of Si_5H and Si_7H are expected to be metastable compared to those predicted by Gupte and Prasad [38].

The Si_lH series of structures displays some special features. It is found that the hydrogen atom in each of them resides outside the framework of silicon atoms being nearly equidistantly positioned from its closest neighbors. However any interaction between them is expected to be weak since the mutual distances are much greater than that of Si-H covalent bond. This was conclusively proved in the vibrational frequency spectrum studies [18]. These structures are also found to be quite sensitive to small energy changes. Thus a energy difference of 0.008 ev is enough to change the geometry drastically from the ground state of Si_7H.

Further studies on these clusters and their derivatives are required to improve our understanding about such emerging materials. Thus using the ground state results, molecular dynamics simulation can be conducted to get an inkling about the various physical and chemical properties of these clusters. It is expected to facilitate the understanding of hydrogen-induced effects in a-Si:H as mentioned previously. This work also establishes the effectiveness of GA in obtaining the ground state structures with much reduced computational efforts. This can be extended further by parallelizing the code for genetic algorithm. A successful venture is expected to open newer vistas of research, especially in the fields of materials simulation and nanostructures a subject of immense importance for the future.

Appendix A

Coordinates of Different Si-H Clusters

Table A.1: SiH_2

Atom	X-Coordinate	Y-Coordinate	Z-Coordinate
Si_1	2.9402	3.0300	0.2400
H_2	2.2201	1.7099	0.0510
H_3	4.3197	2.3700	0.1500

Table A.2: Si_2H

Atom	X-Coordinate	Y-Coordinate	Z-Coordinate
Si_1	1.4471	0.1653	2.2582
Si_2	1.7649	1.1057	0.1188
H_3	1.8940	2.4590	0.8470

Table A.3: SiH_3

Atom	X-Coordinate	Y-Coordinate	Z-Coordinate
Si_1	1.6280	2.4889	1.5420
H_2	0.3051	1.9960	1.0330
H_3	1.8550	3.8429	0.9470
H_4	2.7008	1.5891	0.9940

Table A.4: SiH_4

Atom	X-Coordinate	Y-Coordinate	Z-Coordinate
Si_1	1.4212	1.3712	1.3710
H_2	0.4821	2.3718	0.7910
H_3	2.2479	2.0380	2.4090
H_4	2.3717	0.8520	0.3460
H_5	0.6550	0.2590	1.9760

Table A.5: Si_2H_2

Atom	X-Coordinate	Y-Coordinate	Z-Coordinate
Si_1	2.5018	1.4980	3.1750
Si_2	2.5490	1.4980	0.8560
H_3	1.4981	2.6630	2.9870
H_4	1.3491	0.4730	2.9990

Table A.6: Si_2H_3

Atom	X-Coordinate	Y-Coordinate	Z-Coordinate
Si_1	1.4580	0.3341	1.7790
Si_2	1.7909	2.7299	0.2840
H_3	2.7051	0.0000	0 .9760
H_4	1.9760	2.0010	1.9640
H_5	0.7910	1.1611	0.4199

Table A.7: Si_2H_4

Atom	X-Coordinate	Y-Coordinate	Z-Coordinate
Si_1	3.4830	1.4381	1.8690
Si_2	4.7360	3.4441	3.4541
H_3	4.9320	4.3838	2.2700
H_4	3.1310	2.7790	2.9940
H_5	5.0001	1.8201	2.6520
H_6	3.7569	2.3190	0.6649

Table A.8: Si_2H_5

Atom	X-Coordinate	Y-Coordinate	Z-Coordinate
Si_1	1.0759	1.3008	1.7907
Si_2	3.4540	2.9353	2.5930
H_3	2.6711	1.2432	1.8201
H_4	3.7380	4.0698	1.6140
H_5	2.9160	3.9238	3.6400
H_6	0.8219	1.9082	3.1411
H_7	0.7240	2.3390	0.7342

Table A.9: Si_3H

Atom	X-Coordinate	Y-Coordinate	Z-Coordinate
Si_1	1.9589	2.2518	4.5510
Si_2	2.2459	2.7508	1.8360
Si_3	0.8394	1.1204	2.8041
H_4	3.0969	3.0030	3.4129

Table A.10: Si_4H

Atom	X-Coordinate	Y-Coordinate	Z-Coordinate
Si_1	3.2940	4.6274	2.7843
Si_2	3.9805	2.4705	3.4510
Si_3	1.0783	4.7059	2.0392
Si_4	1.8627	2.5296	2.4118
H_5	4.7647	2.1373	2.1765

Table A.11: Si_5H

Atom	X-Coordinate	Y-Coordinate	Z-Coordinate
Si_1	3.2314	3.5137	1.9610
Si_2	3.1370	0.8785	1.5216
Si_3	1.3491	2.5096	1.0664
Si_4	1.2863	2.1802	3.4197
Si_5	3.6707	1.9451	3.6235
H_6	1.7569	0.4866	2.6510

Table A.12: Si_6H

Atom	X-Coordinate	Y-Coordinate	Z-Coordinate
Si_1	1.0165	1.3637	2.8690
Si_2	4.4770	2.6540	1.5836
Si_3	1.8817	3.5875	2.8104
Si_4	2.5367	1.3294	1.0215
Si_5	3.3187	1.4467	3.4409
Si_6	4.0909	3.6950	3.7047
H_7	2.4976	3.3089	1.1143

Table A.13: Si_7H

Atom	X-Coordinate	Y-Coordinate	Z-Coordinate
Si_1	4.9506	3.7401	4.0978
Si_2	2.9487	3.7431	5.4373
Si_3	1.3131	3.1979	3.4148
Si_4	1.3073	5.2555	4.6048
Si_5	3.3093	5.3112	3.3297
Si_6	2.9927	1.6795	4.1973
Si_7	4.0948	2.5032	2.2599
H_8	2.6937	3.8339	2.1690

Table A.14: Si_8H

Atom	X-Coordinate	Y-Coordinate	Z-Coordinate
Si_1	1.6539	3.1730	3.2434
Si_2	5.4780	3.0264	1.9883
Si_3	5.2962	2.1173	4.1701
Si_4	2.9384	3.7712	1.3431
Si_5	4.0117	1.8182	0.6099
Si_6	4.6334	5.2611	2.1466
Si_7	3.3548	1.5190	2.8915
Si_8	3.5543	3.6892	4.5865
H_9	4.1760	5.1554	3.8123

Appendix B

Structural Details of Si-H Clusters

Table B.1: SiH_2

Bond	Bond Length	Angle	Bond Angle
$Si_1 - H_2$	1.5144	$H_2 - Si_1 - H_3$	92.62
$Si_1 - H_3$	1.5319	$H_2 - H_3 - Si_1$	44.00
$H_2 - H_3$	2.2027	$H_3 - H_2 - Si_1$	43.38

Table B.2: SiH_3

Bond	Bond Length	Angle	Bond Angle
$Si_1 - H_2$	1.5007	$H_2 - Si_1 - H_3$	107.22
$Si_1 - H_3$	1.4962	$H_2 - Si_1 - H_4$	107.98
$Si_1 - H_4$	1.5036	$H_3 - Si_1 - H_4$	106.76
$H_2 - H_3$	2.4125	$H_3 - H_2 - Si_1$	36.33
$H_2 - H_4$	2.4303	$H_4 - H_2 - Si_1$	36.04
$H_3 - H_4$	2.4078	$H_2 - H_3 - Si_1$	36.45

Table B.3: SiH_4

Bond	Bond Length	Angle	Bond Angle
$Si_1 - H_2$	1.4898	$H_2 - Si_1 - H_3$	108.75
$Si_1 - H_3$	1.4851	$H_2 - Si_1 - H_4$	111.59
$Si_1 - H_4$	1.4911	$H_2 - Si_1 - H_5$	109.73
$Si_1 - H_5$	1.4799	$H_3 - Si_1 - H_4$	106.37
$H_2 - H_3$	2.4181	$H_3 - Si_1 - H_5$	109.86
$H_2 - H_4$	2.4655	$H_4 - Si_1 - H_5$	110.45
$H_2 - H_5$	2.4286	$H_2 - H_3 - H_4$	61.79
$H_3 - H_4$	2.3828	$H_2 - H_4 - H_5$	59.34

Table B.4: Si_2H

Bond	Bond Length	Angle	Bond Angle
$Si_1 - Si_2$	2.3406	$Si_2 - Si_1 - H_3$	85.95
$Si_1 - H_3$	1.5451	$Si_1 - Si_2 - H_3$	34.63
$Si_2 - H_3$	2.7121	$Si_1 - H_3 - Si_2$	59.54

Table B.5: Si_2H_2

Bond	Bond Length	Angle	Bond Angle
$Si_1 - Si_2$	2.3194	$Si_2 - Si_1 - H_3$	83.79
$Si_1 - H_3$	1.5492	$Si_2 - Si_1 - H_4$	84.36
$Si_1 - H_4$	1.5525	$H_3 - Si_1 - H_4$	90.09
$Si_2 - H_3$	2.6463	$H_3 - Si_2 - Si_1$	35.59
$Si_2 - H_4$	2.6613	$H_3 - Si_2 - H_4$	48.86
$H_3 - H_4$	2.1950	$H_4 - Si_2 - H_3$	35.49

Table B.6: Si_2H_3

Bond	Bond Length	Angle	Bond Angle
$Si_1 - Si_2$	2.8436	$Si_2 - Si_1 - H_3$	79.13
$Si_1 - H_3$	1.5204	$Si_2 - Si_1 - H_4$	38.81
$Si_1 - H_4$	1.7533	$Si_2 - Si_1 - H_5$	39.39
$Si_1 - H_5$	1.7251	$H_3 - Si_1 - H_4$	91.27
$Si_2 - H_3$	2.9610	$H_3 - Si_1 - H_5$	90.36
$Si_2 - H_4$	1.8406	$H_4 - Si_1 - H_5$	75.04
$Si_2 - H_5$	1.8654	$H_3 - Si_2 - H_5$	51.17
$H_3 - H_4$	2.3477	$H_4 - Si_2 - H_5$	69.78

Table B.7: Si_2H_4

Bond	Bond Length	Angle	Bond Angle
$Si_1 - Si_2$	2.8472	$Si_2 - Si_1 - H_3$	27.39
$Si_1 - H_3$	3.3072	$Si_2 - Si_1 - H_4$	37.52
$Si_1 - H_4$	1.7854	$Si_2 - Si_1 - H_5$	38.31
$Si_1 - H_5$	1.7494	$Si_2 - Si_1 - H_6$	87.32
$Si_1 - H_6$	1.5168	$H_3 - Si_1 - H_4$	48.78
$Si_2 - H_3$	1.5243	$H_3 - Si_1 - H_5$	51.05
$Si_2 - H_4$	1.7972	$H_3 - Si_1 - H_6$	59.99
$Si_2 - H_5$	1.8304	$H_4 - Si_1 - H_5$	74.03
$Si_2 - H_6$	3.1629	$H_4 - Si_1 - H_6$	95.72

Table B.8: Si_2H_5

Bond	Bond Length	Angle	Bond Angle
$Si_1 - Si_2$	2.9951	$Si_2 - Si_1 - H_3$	38.87
$Si_1 - H_3$	1.5965	$Si_2 - Si_1 - H_4$	21.50
$Si_1 - H_4$	3.8451	$Si_2 - Si_1 - H_5$	23.68
$Si_1 - H_5$	3.6994	$Si_2 - Si_1 - H_6$	70.90
$Si_1 - H_6$	1.5023	$H_7 - Si_1 - Si_2$	89.84
$Si_1 - H_7$	1.5225	$H_3 - Si_1 - H_4$	48.32
$Si_2 - H_3$	2.0184	$H_3 - Si_1 - H_5$	61.28
$Si_2 - H_4$	1.5251	$H_3 - Si_1 - H_6$	99.61
$Si_2 - H_5$	1.5370	$H_3 - Si_1 - H_7$	105.56
$Si_2 - H_6$	2.8780	$H_4 - Si_2 - H_3$	116.74
$Si_2 - H_7$	3.3561	$H_4 - Si_2 - H_5$	91.38

Table B.9: Si_3H

Bond	Bond Length	Angle	Bond Angle
$Si_1 - Si_2$	2.7753	$Si_2 - Si_1 - Si_3$	53.98
$Si_1 - Si_3$	2.3632	$Si_2 - Si_1 - H_4$	39.72
$Si_1 - H_4$	1.7761	$Si_3 - Si_1 - H_4$	91.85
$Si_2 - Si_3$	2.3609	$Si_1 - Si_2 - H_4$	38.85
$Si_2 - H_4$	1.8095	$Si_3 - Si_2 - H_4$	91.09
$Si_3 - H_4$	3.0018	$Si_1 - Si_3 - H_4$	36.25

Table B.12: Si_6H

Bond	Bond Length	Angle	Bond Angle
$Si_1 - Si_2$	3.9105	$Si_2 - Si_1 - Si_3$	50.49
$Si_1 - Si_3$	2.3869	$Si_2 - Si_1 - Si_4$	35.78
$Si_1 - Si_4$	2.3928	$Si_2 - Si_1 - Si_5$	37.75
$Si_1 - Si_5$	2.3736	$Si_2 - Si_1 - Si_6$	35.47
$Si_2 - Si_3$	3.0185	$Si_2 - Si_1 - H_7$	32.81
$Si_2 - Si_4$	2.4156	$Si_3 - Si_1 - Si_4$	76.35
$Si_2 - Si_5$	2.4997	$Si_3 - Si_1 - Si_5$	67.77
$Si_2 - Si_6$	2.3941	$Si_3 - Si_1 - Si_6$	34.18
$Si_3 - Si_4$	2.9542	$Si_3 - Si_1 - H_7$	37.34
$Si_3 - Si_5$	2.6543	$Si_4 - Si_1 - Si_5$	64.55
$Si_3 - Si_6$	2.3858	$Si_4 - Si_1 - Si_6$	71.16
$Si_4 - Si_5$	2.5453	$Si_4 - Si_1 - H_7$	41.09
$Si_4 - Si_6$	2.3917	$Si_5 - Si_1 - Si_6$	34.21
$Si_1 - H_7$	3.0094	$Si_5 - Si_1 - H_7$	68.93
$Si_2 - H_7$	2.1370	$Si_6 - Si_1 - H_7$	50.09
$Si_3 - H_7$	1.8257	$Si_1 - Si_2 - Si_3$	37.59
$Si_4 - H_7$	1.9820	$Si_1 - Si_2 - Si_4$	35.39
$Si_5 - H_7$	3.0911	$Si_1 - Si_2 - Si_5$	35.54
$Si_6 - H_7$	3.0656	$Si_1 - Si_2 - Si_6$	73.11

Table B.13: Si_7H

Bond	Bond Length	Angle	Bond Angle
$Si_1 - Si_2$	2.4088	$Si_2 - Si_1 - Si_3$	45.05
$Si_1 - Si_3$	3.7406	$Si_2 - Si_1 - Si_4$	33.65
$Si_1 - Si_4$	3.9784	$Si_2 - Si_1 - Si_5$	66.95
$Si_1 - Si_5$	2.3984	$Si_2 - Si_1 - Si_6$	53.79
$Si_1 - Si_6$	2.8442	$Si_2 - Si_1 - Si_7$	97.55
$Si_1 - Si_7$	2.3749	$Si_2 - Si_1 - H_8$	74.31
$Si_1 - H_8$	2.9702	$Si_3 - Si_1 - Si_4$	35.70
$Si_2 - Si_3$	2.65761	$Si_3 - Si_1 - Si_5$	51.02
$Si_2 - Si_4$	2.3821	$Si_3 - Si_1 - Si_6$	39.81
$Si_2 - Si_5$	2.6516	$Si_3 - Si_1 - Si_7$	55.44
$Si_2 - Si_6$	2.4078	$Si_3 - Si_1 - H_8$	31.47
$Si_2 - Si_7$	3.5981	$Si_4 - Si_1 - Si_5$	33.34
$Si_2 - H_8$	3.2794	$Si_4 - Si_1 - Si_6$	68.96
$Si_3 - Si_4$	2.3770	$Si_4 - Si_1 - Si_7$	88.10
$Si_3 - Si_5$	2.9082	$Si_4 - Si_1 - H_8$	51.31
$Si_3 - Si_6$	2.3956	$Si_5 - Si_1 - Si_6$	90.84
$Si_3 - Si_7$	3.0909	$Si_5 - Si_1 - Si_7$	81.18
$Si_3 - H_8$	1.9653	$Si_5 - Si_1 - H_8$	41.52
$Si_4 - Si_5$	2.3742	$Si_6 - Si_1 - Si_7$	53.24
$Si_4 - Si_6$	3.9742	$Si_6 - Si_1 - H_8$	61.48
$Si_4 - Si_7$	4.5655	$Si_7 - Si_1 - H_8$	40.55
$Si_4 - H_8$	3.1426	$Si_1 - Si_2 - Si_3$	95.05
$Si_5 - Si_6$	3.7473	$Si_1 - Si_2 - Si_4$	112.28
$Si_5 - Si_7$	3.1059	$Si_1 - Si_2 - Si_5$	56.34
$Si_5 - H_8$	1.9770	$Si_1 - Si_2 - Si_6$	72.39
$Si_6 - Si_7$	2.3763	$Si_1 - Si_2 - Si_7$	40.87
$Si_6 - H_8$	2.9740	$Si_1 - Si_2 - H_8$	60.69
$Si_7 - H_8$	1.9344	$Si_3 - Si_2 - Si_4$	55.96

Table B.14: Si_8H

Bond	Bond Length	Angle	Bond Angle
$Si_1 - Si_2$	4.0275	$Si_2 - Si_1 - Si_3$	34.74
$Si_1 - Si_3$	3.9038	$Si_2 - Si_1 - Si_4$	40.96
$Si_1 - Si_4$	2.3704	$Si_2 - Si_1 - Si_5$	34.79
$Si_1 - Si_5$	3.7855	$Si_2 - Si_1 - Si_6$	35.47
$Si_1 - Si_6$	3.8000	$Si_2 - Si_1 - Si_7$	41.91
$Si_1 - Si_7$	2.3985	$Si_2 - Si_1 - Si_8$	55.00
$Si_1 - Si_8$	2.3836	$Si_2 - Si_1 - H_9$	48.82
$Si_1 - H_9$	3.2579	$Si_3 - Si_1 - Si_4$	75.70
$Si_2 - Si_3$	2.3706	$Si_3 - Si_1 - Si_5$	59.15
$Si_2 - Si_4$	2.7241	$Si_3 - Si_1 - Si_6$	59.04
$Si_2 - Si_5$	2.3472	$Si_3 - Si_1 - Si_7$	35.58
$Si_2 - Si_6$	2.3942	$Si_3 - Si_1 - Si_8$	35.01
$Si_2 - Si_7$	2.7560	$Si_3 - Si_1 - H_9$	53.19
$Si_2 - Si_8$	3.3001	$Si_4 - Si_1 - Si_5$	36.41
$Si_2 - H_9$	3.0912	$Si_4 - Si_1 - Si_6$	37.35
$Si_3 - Si_4$	4.0356	$Si_4 - Si_1 - Si_7$	70.86
$Si_3 - Si_5$	3.7966	$Si_4 - Si_1 - Si_8$	88.00
$Si_3 - Si_6$	3.7969	$Si_4 - Si_1 - H_9$	64.34
$Si_3 - Si_7$	2.4004	$Si_5 - Si_1 - Si_6$	60.50
$Si_3 - Si_8$	2.3829	$Si_5 - Si_1 - Si_7$	37.76
$Si_3 - H_9$	3.2578	$Si_5 - Si_1 - Si_8$	88.45
$Si_4 - Si_5$	2.3461	$Si_5 - Si_1 - H_9$	81.78
$Si_4 - Si_6$	2.3955	$Si_6 - Si_1 - Si_7$	77.32
$Si_4 - Si_7$	2.7646	$Si_6 - Si_1 - Si_8$	54.45
$Si_4 - Si_8$	3.3023	$Si_6 - Si_1 - H_9$	27.01
$Si_4 - H_9$	3.0894	$Si_7 - Si_1 - Si_8$	70.53
$Si_5 - Si_6$	3.8212	$Si_7 - Si_1 - H_9$	84.05
$Si_5 - Si_7$	2.3930	$Si_8 - Si_1 - H_9$	32.08
$Si_5 - Si_8$	4.4185	$Si_1 - Si_2 - Si_3$	69.78
$Si_5 - H_9$	4.6281	$Si_1 - Si_2 - Si_4$	34.78
$Si_6 - Si_7$	4.0240	$Si_1 - Si_2 - Si_5$	66.96
$Si_6 - Si_8$	3.0965	$Si_1 - Si_2 - Si_6$	67.07
$Si_6 - H_9$	1.7306	$Si_1 - Si_2 - Si_7$	35.54
$Si_7 - Si_8$	2.7609	$Si_1 - Si_2 - Si_8$	36.28
$Si_7 - H_9$	3.8400	$Si_1 - Si_2 - H_9$	52.49
$Si_8 - H_9$	1.7708	$Si_3 - Si_2 - Si_4$	104.56

References

[1] D.E. Carlson and C.R. Wronski, *Appl. Physics Lett.*, **28** (1976) 671.

[2] P.G. LeComber, *J. Non-Cryst. Solids*, **114** (1989) 1.

[3] J. Kanicki (ed.), Amorphous and Microcrystalline Semiconductor Devices: Optoelectronic Devices, Artech House Inc., (1991).

[4] M. Yamano and H. Takesada,*J. Non-Cryst. Solids*, **77-78** (1985) 1383.

[5] K. Tanaka (ed.), Glow-Discharge Hydrogenated Amorphous Silicon, KTK Scientific Publishers, (1989).

[6] D.L. Staebler and C.R. Wronski, *Appl. Phys. Lett.*, **31** (1977) 292.

[7] W. Luft and Y. S. Tsuo, Hydrogenated Amorphous Silicon-alloy Deposition Process, Marcell Dekker Inc., (1993).

[8] C.C. Tsai, M.. Stutzmann and W.B. Jackson, *Amer. Inst. Phys. Conf. Proc.*, **120** (1984) 242.

[9] S.R. Kurtz, Y.S. Tsuo and R. Tsu, *Appl. Phys. Lett.*, **49** (1986) 951.

[10] S.R. Eliot, *Phil. Mag.*, **B39** (1979) 349.

[11] M. Stutzmann, W.B. Jackson and C.C. Tsai, *Phys. Rev. B*, **32** (1985) 23.

[12] H. Dersch, J. Stuke and J. Beichler, *Appl. Phys. Lett.*, **38** (1980) 456.

[13] D. Adler, *Solar Cells*, 9 (1983) 133.

[14] Y. Bar-Yam, D. Adler, and J.D. Joannopoulos, *Phys. Rev. Lett.*, **57** (1986) 467.

[15] H.M. Branz and M. Silver, *Phys. Rev. B*, **41** (1990) 7887.

[16] D. Redfield and R.H. Bube, *Phys. Rev. Lett.*, **65** (1989) 464.

[17] M. Menon and K.R. Subbaswamy, *Phys. Rev. B*, **47** (1993) 12754.

[18] G.R. Gupte and R. Prasad, *Int. J. Mod. Phys. B, 12(15)* (1998) 1607.

[19] D.E. Goldberg, Genetic Algorithms in Search, Optimization, and Machine Learning, Addison-Wesley, (1989).

[20] K. Deb, Optimization for Engineering Design Algorithms and Examples, Prentice Hall India, (1996).

[21] D.E. Goldberg and K. Deb, " A comparative analysis of selection schemes used in Genetic Algorithm", TCGA Report No. 9007, Deptt. of Engg. Mechanics, University of Alabama, (1990).

[22] Melannie Mitchell, An Introduction to Genetic Algorithms, Prentice Hall of India Pvt. Ltd., (1998).

[23] Q. Xiaofeng and F. Palmieri, *IEEE Trans. Neural Networks*, **5(1)** (1994) 120.

[24] D.E. Goldberg and J. Richardson, "Genetic Algorithm in Sharing for multimodal function optimization", in J.J. Grefensette ed., Genetic Algorithms and their Applications: Proceedings of the Second International Conference on Genetic Algorithms, Erlbaum, (1987), 41.

[25] K. Deb and D.E. Goldberg, "An investigation of niche and species formation in genetic function optimization", in J.D. Schaffer ed., Proceedings of the Third International Conference on Genetic Algorithms, Morgan Kaufmann, (1989).

[26] K. Krishnakumar, *Intelligent Control and Adaptive Systems*, SPIE Vol. 1196 (1989).

[27] K. Price and R. Storn, *Dr. Dobb's Journal.*, **22** (1997), 18.

[28] W. Kohn and L.J. Sham, *Phys. Rev. A* , **140** (1965) 1133.

[29] M. van Schilfgarde and W.A. Harrison, *J. Phys. Chem. Solids*, **46** (1985) 1093.

[30] W.A. Harrison, Electronic Structure and Properties of Solids, Freeman San Fransisco, (1980).

[31] M. Menon and K.R. Subbaswamy, *Phys. Rev. B*, **50** (1994) 11577.

[32] D. Caroll, Developments in Theoretical and Applied Mechanics, Vol.XVIII ed. H.B. Wilson, C.W. Batra, A.M. Bert, T.A. Schapery, D.S. Stewart, F.F. Swinson, School of Engineering, University of Alabama, U.S.A, (1996).

[33] K. Deb and N. Chakraborti, "A Combined Heat Transfer and Genetic Algorithm Modeling of an Integrated Steel Plant Bloom Re-heating Furnace", Proceedings 6th European Congress on Intelligent Techniques & Soft Computing (EUFIT'98), Aachen, Germany, Sept. 7-10, Verlag und Druk Mainz GmbH, Aachen, Germany (1998).

[34] I. Dubois, *Can. J. Phys.*, **46** (1968) 2485.

[35] W.D. Allen and H.F. Schaefer, *Chem. Phys.*, **108** (1986) 243.

[36] H.W. Kattenberg and A. Oskam, *J. Mole. Spectrosc.*, **49** (1974) 52.

[37] A.B. Sannigrahi and P.K. Nandi, *Chem. Phys. Lett.*, **188** (1992) 575.

[38] G.R. Gupte and R. Prasad, *Int. J. Mod. Phys. B*, **12(16-17)** (1998) 1737.

[39] K. Raghavachari and C.M. Rohlfing, *J. Chem. Phys.*, **89(4)** (1988) 2219.